On the role of a large shallow lake (Lake St. Clair, USA-Canada) in modulating phosphorus loads to Lake Erie

Serghei A. Bocaniov[1, 2,*], Philippe Van Cappellen[2], and Donald Scavia[3]

[1] Graham Sustainability Institute, University of Michigan, Ann Arbor, Michigan, USA.

[2] Department of Earth and Environmental Sciences, University of Waterloo, Waterloo, Ontario, Canada.

[3] School for Environment and Sustainability, University of Michigan, Ann Arbor, Michigan, USA.

* Corresponding author: sbocaniov@waterloo.ca

Abstract

It is often assumed that large shallow water bodies are net non-depositional and that if they have multiple nutrient loads, those loads are quickly homogenized before exiting the water body. While this may be true for some systems, where it is not, it has impacts for understanding and predicting consequences of nutrient load reductions, both for the water body and for those downstream of it. We used a previously calibrated and validated three-dimensional hydrodynamic water quality model of a large shallow lake, Lake St. Clair (US/Canada), to quantify the total and dissolved phosphorus (TP and DRP) transport and retention, and construct tributary-specific relationships between phosphorus load and the amount that leaves the lake for the three major tributaries. Lake St. Clair is situated between the St. Clair and Detroit rivers that feed Lake Erie. Efforts to reduce Lake Erie's re-eutrophication requires an understanding of nutrient transport and retention in each of its sub-watersheds including those that feed indirectly via Lake St. Clair. We found that over the simulation period, the lake retained a significant portion of TP (17%) and DRP (35%) load, and that TP retention is spatially variable and largely controlled by a combination of lake depth and wind-induced resuspension. Compared to the Clinton and Sydenham rivers, the Thames river contributed a larger proportion of its load to the lake's outflow. However, because the lake's load is dominated by the St. Clair River, 40% reductions of nutrients from those sub-watersheds result in less than 5% reduction from the lake.

1. Introduction

While impacts of harmful algal blooms (HABs) and hypoxia were once reduced significantly in the Great Lakes, they have resurfaced, particularly in Lake Erie (Scavia *et al.*, 2014). Under the 1978 binational Great Lakes Water Quality Agreement (GLWQA) (IJC, 1978), reductions in point sources of phosphorus (P) loads resulted in a 50% reduction in total P (TP) loading, with associated improvements in water quality and fisheries (Charlton et al., 1993; Ludsin et al., 2001). However, with changes in the ecology, climate, and the now dominant nonpoint P sources, Lake Erie's HAB and hypoxia extent and duration increased dramatically since the mid-1990s (Bridgeman et al., 2013; Scavia et al., 2014). The hypoxic area is now often comparable to the 1970s, with a new record size set in 2012 (Zhou et al., 2015) reaching a maximum daily extent of 11,600 km^2 (Karatayev et al., 2018), and toxic *Microcystis* blooms set records in 2011 (Michalak et al., 2013) and 2015, and the 2014 bloom led to a "do not drink" advisory for 500,000 people living in the Toledo, Ohio area. In response to these changes, the U.S. and Canada revised Lake Erie's loading targets (GLWQA, 2016; IJC, 2012), based largely on science input from a multi-model effort (Scavia et al., 2016) and a public review process. The new targets call for reducing annual and spring (March-July) P loads to Lake Erie by 40 percent from their 2008 levels for west and central basins, while those for the east basin are still being developed and will be finalized in 2020. The task ahead is to develop and implement Domestic Action Plans (IJC, 2017) that achieve that reduction, primarily from the now dominant and harder to treat nonpoint sources.

The plans will undoubtedly address loads from all sources, but because the Detroit and Maumee rivers contribute 41% and 48% of the total P (TP) load and 59% and 31% of the dissolved reactive P (DRP), respectively (Maccoux et al., 2016; Scavia et al., 2016, 2019), they

will likely get special attention. Several efforts are in place to assess the relative contributions of, and potential controls of, P loads from the Maumee River watershed (e.g., Scavia et al., 2017; Muenich et al., 2016; Kalcic et al., 2016). Similar efforts are in place for the binational watersheds of the connecting channel between Lake Huron and Lake Erie (Scavia et al., 2019; Hu et al., 2018; Bocaniov and Scavia, 2018; Dagnew et al., in review), but unlike the Maumee watershed, much of the connecting channel P loads do not flow directly into Lake Erie. Much of it must pass through the relatively large Lake St. Clair (Fig. 1a) that has its own sizable watershed consisting of both highly urbanized areas (e.g. Detroit, Windsor, London) and watersheds (e.g. Clinton river basin), as well as intensive agriculture in the Thames and Sydenham river basins.

The average relative phosphorus loads to Lake St. Clair for 2013-2015 are 71.5%, 4.8%, 12.1%, and 5.4% from the connecting channel inflow (St. Clair River) and three major tributaries, Clinton, Thames, and Sydenham rivers, respectively (Scavia et al., 2019). Because these are substantial inputs to the overall system, and because Scavia et al. (2019) estimate that Lake St. Clair retains, on average, 20% of its TP inputs, it is important to understand how P load reductions from individual tributaries to Lake St. Clair will correspond to the reduction in load to Lake Erie via the Detroit River.

Here, we used a previously calibrated and validated ecological model of Lake St. Clair (Bocaniov and Scavia, 2018) to explore drivers of the nutrient attenuation capacity of Lake St. Clair and explore the sensitivity of nutrients leaving the lake to modifications in loads from each of its three major tributaries.

2. Methods

2.1 Study Site – Lake St. Clair is an integral part of the Laurentian Great Lakes system shared by Canada and the United States. However, in contrast to the Great Lakes proper, it is small (1114 km^2, 4.3 km^3) shallow (mean depth 3.9 m; Table 1; Fig 1b), with short theoretical water residence time (~9 days) and the largest ratio of watershed to lake surface area (13.8; =15400/1114) among all other lakes in the Great Lakes - Laurentian River Basin (Bocaniov and Scavia, 2018; Table 2). Its watershed is one of the most densely populated in the Great Lakes region, and this binational lake is an important source of drinking water, commercial and sport fishing, and other forms of recreation. Located in the connecting channel between Lakes Huron and Erie, the lake processes water from the upper Great Lakes (Superior, Michigan, Huron) via the St. Clair River, as well as from its proximate 15,400 km^2 watershed that is roughly 63% in Canada and 37% in the United States (Table 2). In addition to receiving P from the upper Great Lakes and the watersheds of the St. Clair River, it receives P from many direct tributaries, including significant loads from the Clinton, Thames, and Sydenham rivers, as well as point source discharges (Scavia et al., 2019). While the lake's theoretical flushing time is roughly 9 days, that flushing time (or water residence time) varies seasonally and, more significantly, spatially (Bocaniov and Scavia, 2018) such that during summer, water in the south-eastern part of the lake flushes more slowly than water in the north-western part. This, in combination with different timing and magnitude of tributary loads, leads to spatial segmentation of primary production resulting in the northwest part of the lake being oligotrophic and southeast part mesotrophic (Bocaniov and Scavia, 2018).

2.2 River discharges – Characteristics of the sub-watersheds and daily flows (Tables 2-3) of the main inflow (St. Clair River), three major lake tributaries, and other smaller tributaries (Table 3;

Fig. 1a) follow Bocaniov and Scavia (2018) and Scavia et al. (2019). Details of calculations and information on gauging stations can be found in Table S6 in Bocaniov and Scavia (2018) and Table S1 in Scavia et al. (2019). In brief, we downloaded data from the United States Geological Survey (USGS) National Water Information System (https://waterdata.usgs.gov/nwis) for the US sites and from the National Water Data Archive: HYDAT (http://tinyurl.com/y8be92pz) for sites in Canada. For tributaries with multiple upstream flow gauges (e.g. the Sydenham river), we used area-weighted calculations to estimate flow at the downstream confluence. Similar to Scavia et al. (2019), flow values for tributaries without long-term flow gauges were estimated using area-weighted method based on values from nearby streams with flow gauges. To account for the most typical pattern in inter-annual hydrograph conditions in major lake tributaries (Thames, Sydenham, and Clinton Rivers), as well as to reduce the noise from the inter-annual variability in river discharge from these tributaries, we averaged daily values of river discharge over the past 17 years (2000 to 2016). Because the St. Clair River discharge varies little from year to year, we used values from 2009 (Bocaniov and Scavia, 2018).

2.3 Meteorological, wave, water level and bottom currents data - For model simulations (2009) and our analysis of seasonal/inter-annual patterns in wind speeds and directions (2009 and 2010) we used meteorological observations collected at Detroit City Airport (Detroit, MI; 42.41°N, 83.01°W; anemometer height: 10 m above site elevation). The meteorological data were corrected to account for the open water conditions as in Bocaniov and Scavia (2018). For analysis of open water wave conditions (wave heights and periods), we used data collected during the seasonal buoy moorings (station #45147; Table ST-1) deployed in the middle of the lake (Fig. 1a) at 6 m depth and maintained by Environment and Climate Change Canada

(ECCC). Water level data were analyzed based on observations at three gauging stations (Fig. 1a; Table ST-1): #9034052, # 9044049, and #11965. Water level data along with the lake bathymetry were used to calculate the representative lake volumes, mean and maximum depths, and allocation of bottom area into zones of similar depth with increments of about 1 m.

Because bottom current observations were not available for 2009, we assumed data from ECCC's 2016 Doppler Current Profiler (ADCP) deployments were representative. The two ADCPs (stations A1-2; Fig. 1a; Table ST-1) were deployed in the south-eastern part of the lake from April 27 to November 3, and focused on near-bottom currents, their dynamics and characteristics. They were deployed at 0.5 m (A1) and 0.6 m (A2) above bottom and mounted on the bottom and configured as upward looking.

2.4 The Model - We used the three dimensional (3D) coupled hydrodynamic and ecological model previously applied to Lake St. Clair (Bocaniov and Scavia, 2018): The Estuary, Lake and Coastal Ocean Model (ELCOM) driven by the Computational Aquatic Ecosystem DYnamic Model (CAEDYM). ELCOM is a 3D hydrodynamic model that serves as the hydrodynamic driver for CAEDYM, a model capable of simulating a wide range of ecological processes and state variables (Hipsey, 2008; Hipsey and Hamilton, 2008). ELCOM-CAEDYM, with different levels of ecological complexity, has been used widely for large North American lakes, including Lakes Winnipeg, Ontario, Erie and St. Clair, for investigation of different aspects of nutrient and phytoplankton dynamics (e.g. Leon et al., 2011), relationship between transport time scales and nutrient losses (Bocaniov and Scavia, 2018), hypoxia (Bocaniov and Scavia, 2016; Bocaniov et al., 2016), the relative importance of meteorological forcing parameters (e.g. Liu et al., 2014; Bocaniov et al., 2014a), winter conditions (e.g. Oveisy et al., 2014), and the role of mussels in

shaping temporal and spatial pattern of phytoplankton biomass (Bocaniov et al., 2014b) or interactions between hypoxia and spatial distribution of mussels (Karatayev et al., 2018).

For this application, we used the nutrient and phytoplankton components that simulate dynamics of phosphorus, nitrogen, and silica, and five functional groups of phytoplankton as described in Bocaniov et al. (2016) and Bocaniov and Scavia (2018). While this model does not simulate mussels and zooplankton as state variables, their grazing effects on phytoplankton are accounted for in phytoplankton loss rates. More detailed information on CAEDYM, and the specific details of its application to large lakes, is provided in Leon et al. (2011), Bocaniov et al. (2014b; 2016), and Bocaniov and Scavia (2018).

Lake St. Clair bathymetry, initial lake conditions, and meteorological drivers were assembled from the wide range of sources described in Bocaniov and Scavia (2018). The model was run with a computational grid resolution of 500 m × 500 m in horizontal (Fig. 1b) and 0.15 to 0.26 m in vertical dimension at a 5 min time step from March 1 through October 31. The model was calibrated and validated in previous applications (Bocaniov and Scavia, 2018).

2.5 Nutrient loading, retention, and tributary-specific nutrient response curves and retention times. Nutrient loads from the St. Clair River and three major tributaries (Thames, Sydenham and Clinton rivers) were calculated as in Scavia et al. (2019), using daily concentrations averaged over 2013 to 2015 which compared well with estimates from other studies (e.g. Burniston et al., 2018). For all other tributaries, which are minor in terms of flow and nutrient loads, the concentrations were kept as those as in 2009 (Bocaniov and Scavia, 2018).

Lake St. Clair TP and DRP retention for the March 1 through October 31 simulation period was estimated as the difference between the calibrated model's total input and total

amount leaving the lake through the Detroit River, expressed as a percent of the total input. As such, the retention corresponds to TP removed from the system via settling or consumption in the benthos, while the DRP retention corresponds to the amount converted from DRP to particulate organic P through biological uptake and incorporation into phytoplankton biomass, which may either leave the lake via Detroit River or settle and be removed from the water column.

To explore the relative sensitivity of export from Lake St. Clair to changes in tributary loads, we developed tributary-specific response curves for the Clinton, Thames, and Sydenham rivers. For each tributary, one at a time, we ran the model with a range of TP and DRP loads varied from the base load by 50%, 75%, 125% and 150%. The resulting loads leaving Lake St. Clair were plotted against the input loads. Because the load is dominated by the St. Clair River, we used the initial response curve to determine the intercept that was then subtracted from the loads and plotted again to provide a clearer comparison among slopes.

To estimate the lake residence times of river water from the St. Clair River and each of the three major tributaries, we used a conservative tracer in the river inflow and estimated the temporal dynamics of river water residence time as the difference between the accumulated amount of tracer that entered the lake and accumulated amount of tracer leaving the lake via the lake outflow.

To explore the capacity of Lake St. Clair to modify nutrient transport and retention due to inter-annual variability in meteorological drivers, we estimated nutrient retention under different meteorological forcing scenarios, in addition to our basic run (Table 4), using observed meteorological from different years, leaving all other conditions unchanged. To select the additional sets of meteorological conditions, we screened both the meteorological observations and satellite-derived lake surface temperatures between 1995 and 2014 and selected eight years

to represent a wide range in wind speed and air temperature (1995, 1996, 2003, 2005, 2008, 2010, 2012, and 2014; Table 4). For each set of meteorological conditions, we calculated retention of TP (R_{TP}) and DRP (R_{DRP}), and averaged over the entire simulation period air temperature ($\overline{AT}$) and wind speed ($\overline{WS}$). To explore the relationships between nutrient retention and $\overline{AT}$ and $\overline{WS}$) we used ordinary least squares, bivariate or multivariate linear regression models.

2.6. Segmenting the lake into wave-impact depth zones - The segmentation of the lake into zones was based on surface wave length and height. Season-averaged surface wave length (L_o) can be estimated from wave period (T) and for relatively deep water such as that at the location of buoy #45147 (depth 6 m) it can be calculated as in Masselink et al. (2014):

$$L_o = \frac{gT^2}{2\pi} \quad (1)$$

where g is the gravitational constant, and T is season-averaged wave period estimated from measurements at buoy #45147 (Fig. 1a).

To partition the lake into two characteristic depth (D) zones based on the disturbance effect of surface waves on the lake bed we followed Masselink et al. (2014): (i) intermediate and shallow water where the lake bottom is affected by waves: $D/L_o < 0.5$; and, (ii) deep water where the lake bottom is affected by waves: $D/L_o > 0.5$.

2.7 Bottom Shear Stress – Bottom shear stress is caused by action of both wind-driven surface waves and water currents, $\tau_{cw} = \tau_w + \tau_c$. The bottom shear stress due to wind waves (τ_w) was calculated from wave height, period, and length, as in Hawley and Lesht (1992):

$$\tau_w = \frac{H \cdot \rho \cdot \nu^{0.5} \left(\frac{2\pi}{T}\right)^{1.5}}{2\ sinh\left(\frac{D2\pi}{L}\right)} \quad (2)$$

where τ_w is the bottom shear stress due to surface waves (N m^{-2}), H the significant wave height (m; observed), ρ the density of water (kg m^{-3}) and calculated as in Tanaka et al. (2001), υ the kinematic viscosity of water (cm^2 s^{-1}) and calculated as in Kestin et al. (1978), T the wave period (s; observed), D the local water depth (m; observed), and L the wave length calculated from T (m) and calculated as in Dean and Dalrymple (1984).

The bottom current shear stress due to currents (τ_c) is calculated from:

$$\tau_c = \rho \left(\frac{k \cdot u_z}{\ln(z/z_o)}\right)^2 \quad (3)$$

where, k is von Karman's constant (0.41), u_z is average velocity, z is elevation above bed, and z_o is a hydraulic bed roughness length which depends on bed types. The dominant bed type in Lake St. Clair is silty-sand (Hawley and Lesht, 1992), so the typical value of z_o for bed type represented by mixture of silt and sand is 0.005 cm (Soulsby, 1983). To lift sediments into the water column and keep them in suspension, the instantaneous bottom shear stress ($\tau_{cw} = \tau_w + \tau_c$) has to be above the critical shear stress (τ_{crit}). We used τ_{crit} = 0.25 N m^{-2} as estimated by Tsai and Lick (1986) for Lake St. Clair.

3. Results

3.1. Nutrient loads, retention, and response to reductions.

Estimates of flows, nutrient loads, and residence times for major tributary inputs – The St. Clair River was responsible for 97.1% of inflow and 78.1% and 71.9% of the TP and DRP loads, respectively (Table 3). The Thames, Sydenham, and Clinton rivers accounted for roughly 2.1% of lake inflow and 18.8% and 23.5% of the TP and DRP loads. All other tributaries were responsible for about 0.1% of the inflow and 1.3% and 2.8% of the TP and DRP loads, respectively. Over-lake precipitation and atmospheric load of phosphorus load accounted for about 0.7% lake water inflow and 1.7% and 1.8% of the TP and DRP loads, respectively.

Based on conservative tracers released with the St. Clair River and tributary inflows, the St. Clair River had the shortest water residence time (WRT) ranging from 3 to 7 days with a mean value of 5 days. WRTs for the tributaries were short in spring and longer in summer and fall. In spring, WRTs were 8, 11 and 11 days for Clinton, Sydenham, and Thames rivers, respectively. In summer and fall, they increased to 21, 35 and 39 days, respectively. The spatial and temporal distribution of the Thames river water mass shows that it tends to have a strong local effect (Fig. 2) in the vicinity of the Thames river mouth and along the south-east and south shores. The presence of Thames river in locations further offshore was generally small, with the largest values in March and April and then decreasing towards May and June and almost zero in July and following months. Water from the Sydenham River (not shown) generally moved along the north-western part of the lake but was more diluted with the lake water compared to the Thames. Clinton River water (Fig. 3) was diluted and mixed rapidly with the strong flow of the St. Clair River water. Depending on the winds, its waters can be advected into shallow Anchor Bay, and/or L'anse Creuse Bay (Fig.1a).

TP and DRP Retention (R_{TP}, R_{DRP}) and the relation to atmospheric forcing – Lake-scale retention during the simulation period (March 1 to October 30) for the base case (2009; Scenario B; Table 4) was 17.3% for TP (R_{TP}; Table 5) and 34.8% for DRP (R_{DRP}; Table 6). Over the range of meteorological conditions tested (Table 4), average retention (±SD) was 17.8 ±2.3% for R_{TP} (Table 5) and 34.8 ±1.2% (Table 6) for R_{DRP}. R_{TP} was larger during the years with relatively lower winds (Table 5).

Seasonally averaged wind speed ($\overline{WS}$) and air temperature ($\overline{AT}$) for each meteorological forcing scenario are summarized in Tables 5 and 6. $\overline{WS}$ was a better predictor than ($\overline{AT}$) of R_{TP} and R_{DRP} (Table 7). There was a strong and statistically significant negative relationship between $\overline{WS}$ and R_{TP}. While $\overline{AT}$ alone was not a significant variable, it added significantly and positively to the variance already explained by $\overline{WS}$. R_{DRP} was also significantly and negatively related to $\overline{WS}$. Similar to with R_{TP}, $\overline{AT}$ alone was not a good predictor, but it added significantly to the amount of variance already explained by $\overline{WS}$. R_{DRP} and R_{TP} were strongly related and the former can be expressed as a constant value (172 MT) plus 13% of R_{TP}.

Tributary-specific nutrient response curves – All TP and DRP load-response curves were linear (Fig. 4), indicating proportional changes in the nutrient load leaving the lake outflow through the Detroit River as a function of load reductions in the tributaries. For TP (Fig. 4a), the slopes for the Sydenham and Clinton rivers were similar (0.55 and 0.54, respectively) and lower than for the Thames river (0.65). For DRP (Fig. 4b), the Clinton river had a smaller slope (0.53) than for the Thames and Sydenham rivers (0.65 and 0.66, respectively). Consistent with the retention estimates, all slopes were less than 1, indicating that the reduction in total load to the Detroit River was smaller than the reduction of the nutrient load in any of the LSC tributaries.

3.2. Drivers and controls of nutrient retention and load response.

To explore potential mechanisms controlling variation in time and space, among tributaries, and between TP and DRP of retention and response, we analyzed winds, waves, and currents in the context of water levels, bathymetry, and sediment deposition and resuspension.

Winds, waves, and near-bottom currents – Wind frequencies, speed, and directions at the Detroit City Airport meteorological station in 2009 (Figs. SF-1–3) and 2010 (Figs. SF-4–6) followed a seasonal cycle with some inter-annual variability. Winds were more frequent westerly (west and southwest, but also from the northwest) with some exceptions, such as during spring when winds were either blowing equally from all directions or more frequent from the north-east.

Observed wave periods were typically short with median and mean (±SD) values of 2 s and 2.44 ±0.56 s, respectively at buoy #45147 (April 20 to December 7, 2009). Wave heights were typically small (Fig. SF-7), with the most frequent observation (25.3%) being 0.1 m and waves exceeding 0.7 m occurred in less than 1.2% of the observation period. Excluding periods of calm, the median significant wave height was 0.30 m with mean of 0.29 ±0.17 m. While stronger winds generated larger waves in spring and fall, their durations were short lived.

Near-bottom currents measured at stations A1 and A2 ranged from < 1 to 14 and 23 cm s^{-1} during storms (Table ST-2, Figs. SF-8-11), but were typically small and for the depths closest to the bottom, the overall monthly means of 2.5 ±1.5 and 3.7 ±2.7 cm s^{-1} at stations A1 and A2, respectively.

Current- and wave-induced bottom shear stress - Estimated bottom shear stress due to wave action (τ_w) was largely dependent on local depth (Fig. 5). At shallow sites (e.g. 2-4 m; Fig. 5a-c) it frequently approached or exceeded the critical shear stress (τ_{crit} = 0.25 N m^{-2}). While at deeper ($\geq$ 5 m) sites, it could exceed τ_{crit} during storms but was less than τ_{crit} for long periods of time (Fig. 5d-f). Because near-bottom currents were slow, current-related bottom shear stress (τ_c) was small (mean ±SD of 0.005 ±0.007 and 0.013 ±0.023 N m^{-2} for A1 and A2, respectively), typically an order of magnitude smaller than τ_w.

Lake depth and wave disturbing effects – Our analysis of wave characteristics observed at buoy #45147 (Fig. 1a) suggest the lake bed can be characterized as two distinct zones: shallow and intermediate water zone where lake bed is affected by waves ($\leq$ 4.9 m), and deep water zone where lake bed is unaffected by surface waves (depth 5 to 6.4 m) for most of the time. This deep water zone ($\geq$ 5 m) was similar to those depths where the bottom shear stress tended not to exceed τ_{crit} for most of the time (e.g. Fig. 5d-f). Though lake is shallow (Fig. 1b; Table 1), there is a significant portion of the lake bottom area with the depth $\geq$ 5 m (Table 8) accounting for almost 30% of the entire lake area.

4. Discussion

Phosphorus retention - We showed that during March 1 to October 31, the lake was a net sink for phosphorus with an average TP retention under different observed meteorological forcing (Table 4) of about 18% (Table 5). This retention rate estimate is similar to the 1998-2016 average annual retention of 20% estimated with a TP mass balance based on measured loads into and out of the lake (Scavia et al., 2019), and the variability with meteorological conditions (Table

7) may explain the substantial inter-annual variability (4-34%) Scavia et al (2019) reported. The small difference between our estimate and that of Scavia et al. (2019) may be because our simulation period did not include ice-covered season when the lake surface is sheltered from the effects of wind stress and settling rates should dominate resuspension. Our model also did not include rooted aquatic macrophytes, which may attenuate the bottom shear stress and thus reduce the resuspension.

Scavia et al. (2019) concluded that the Lang et al. (1988) estimate of TP retention was underestimated because it was based on an estimated load from Lake Huron and the St. Clair River loads rather than direct measurements into Lake St. Clair, and they showed that those estimates of the Lake Huron loads are underestimates. They also suggested that the discrepancy could be because of the significant dreissenid mussel invasion in the late 1980s (Nalepa et al., 1996). Nalepa et al. (1991) estimated that the mussel-related retention of TP during between May and October was 134 MT, corresponding to about 8.6% of the external TP load during the same period. Lang et al. (1988) estimated macrophyte growth to be on the order of 219 MTA, or roughly 7% of TP loads. So, together these could account for a substantial portion of the retention. However, physical controls also appear important.

Wind-induced control of nutrient retention - While the lake is shallow, with extensive areas where resuspension rates may be comparable to settling rates, there are deeper zones ($\geq$ 5 m; Table 8) where currents and waves (see Table ST-2 and Figs. SF-8-11 ; Fig. SF-7) are not sufficient to generate bottom shear stresses exceeding τ_{crit} (e.g. Fig. 5). In addition, our results show a strong relationship between TP retention and season averaged wind speed (Table 7; models 1 and 3). This is consistent with the fact that more than 70% of the lake bottom is

susceptible to waves (Table 8) and that in relatively shallow lakes the TP dynamics is largely controlled by wind-induced resuspension (e.g. Hamilton and Mitchell, 1996; 1997). We also showed a statistically significant negative relationship between DRP retention and average wind speed, though weaker than that for TP. Hamilton and Mitchell (1997) also found the relationships between DRP and wind-induced bottom shear stress to be considerably weaker than those for TP, and inconsistent across the seven shallow lakes they studied. The stronger relationship for TP is expected because, unlike DRP, particulate phosphorus is controlled primarily by the balance between settling and resuspension, with latter driven by the wind-induced resuspension.

The relationship between R_{DRP} and R_{TP} (Table 7, model 7) suggest that the former is a product of two components. One represents the relatively constant amount of DRP converted to algal biomass and exported via the lake outflow (~172 MT; intercept of model 7). Because this is constant across scenarios, it might suggest that algal production is limited more by flushing than by nutrients and/or light. The second component suggests that DRP retentions is approximately 13% of TP retention, reflecting the amount of DRP incorporated into algal biomass and removed from the water column by settling.

Load-response relationships – While it is common to assume that nutrient loads from different tributaries are mixed homogeneously in the receiving water body and contribute equally and proportionally to the load leaving the lake, our study illustrated that the spatial and temporal processing of individual loadings are important. Therefore, it is important to understand the "spatial-temporal variation" in the effects of tributary loads to help prioritize watersheds that can be most effective in per-unit load reductions.

The DRP response curve slopes (Fig. 4b) ranged from 0.53 to 0.65, indicating that the lake retains 35% to 47% of the tributary DRP loads. Our model suggests for the overall lake retention of DRP 35% (base case; Table 6) which is consistent with the slopes of the Thames and Sydenham river DRP response curves (Fig. 4b). A larger portion of the DRP load to Lake St. Clair comes from Lake Huron (St. Clair River; Table 4) comes in spring when phytoplankton biomass in Lake Huron is still small. For the tributaries with streamflow dominated by snow melt and spring runoff (Thames and Sydenham rivers), a larger portion of DRP is also comes in spring. In spring, Lake St. Clair has a short water residence time, small phytoplankton biomass and insignificant DRP loss, so the DRP load leaves the lake very quickly (Bocaniov and Scavia, 2018). The Clinton river DRP retention is larger than for the overall lake retention and other two major tributaries (47% vs. 35%), because this river drains an urban area with a stable flow pattern and its DRP load of more equally distributed over the season including summer time when temperature, intensity of solar radiation and duration photoperiod, as well as higher phytoplankton biomass are all accelerating the DRP loss via phytoplankton uptake (Bocaniov and Scavia, 2018). A larger similarity between overall lake retention of DRP and those of the tributaries comes from the fact that DRP is a dissolved P and not affected by settling and resuspension processes as TP does.

The slopes of the TP (Fig. 4a) response curves ranged from 0.53 to 0.65, indicating tributary-specific retention rates of 47% to 35% compared to the overall lake retention rate of 17.3% (Table 5). This is likely because over 70% of the load to Lake St. Clair comes from the St. Clair River (Scavia et al., 2019) which has a WRT of 5 days, considerably smaller than those for the tributaries (8-11 days in spring; 21-39 days in summer and fall). The shorter residence time

for St. Clair River water reduces the time available for biological processing of nutrients, reducing the potential for sedimentation and retention compared to the tributary waters.

Based on these export efficiencies, the Thames (0.64) is more efficient in reducing the TP load leaving the lake than the Sydenham (0.55) and the Clinton (0.54). For every 100 MT reduction in the load from the Thames, Sydenham, and Clinton, we would expect 64, 55, and 54 MT less leaving Lake St. Clair, respectively. Based on the DRP efficiencies, the Thames and Sydenham (0.65) are more efficient than the Clinton (0.53). The differences in slopes can be explained by the interactions of lake circulation and wind-induced resuspension, in the context of the seasonal timing of tributary loads.

Thames River water and P load is transported along the shallower south-east and east shore (Figs. 2 and 1b) where TP load that had settled to the lake bed can also be easily re-suspended and moved toward the lake's outflow. In addition, the Thames load is largest in late winter, early spring, and late fall (Fig. 6a-b), coinciding with variable and northeastern winds (Figs. SF-1c-d and SF-4c-d) and circulation pattern favoring flushing (Fig. SF-12d) and shorter river water residence times (~11 days). In late spring and summer, after most of the Thames P load has entered the lake, winds are westerly (e.g. Figs. SF-2a-d and SF-5a-d), with the strongest winds from the northwest driving circulation patterns (Fig. SF-12e-h) that increase Thames water residence times to 30 - 40 days.

While the Sydenham and Thames river hydrograph and DRP retention rates are similar, their TP retention rates differ. The Sydenham is located much further from the lake outflow and separated from it by a basin deep enough ($\geq$ 5 m; Fig. 1a-b) to be net-depositional (e.g. Fig. 5d-f), thus enhancing particulate phosphorus retention resulting in a higher TP retention rate. The presence of the deep basin, however, would not affect DRP dynamics. Because both rivers have

similar hydrographs and short residence times in spring (~11 days) when their DRP load is highest and phytoplankton growth is limited (Bocaniov and Scavia, 2018), DRP is quickly flushed from the lake resulting in similar load-response slopes.

Clinton river TP and DRP load-response curves have smaller slopes than the Thames, indicating larger portions of both are retained by lake. The Clinton River load is more evenly distributed over the year (Fig. 6a-b), therefore a substantial amount of it is delivered during periods of higher production and settling, leading to higher nutrient retention rates. The Clinton River water mass also mixes over a larger area, allowing TP settling not only in the naturally deeper parts of the lake but also the deeper, ~8.4 m navigational channel (Fig. 1b). The load can also be advected to a small bay in the north (Anchor Bay) or to the L'anse Creuse Bay (Fig. 3, 1a) and be trapped there.

While tributary load reductions will result in reduced load leaving the lake, those reductions are likely to be small compared to the overall load. For example, because the average baseline load leaving Lake St. Clair during the simulation was 1597 MT, even 50% reductions in tributary loads will reduce the load leaving the lake by less than 5%. However, it is important to explore their differences because they will likely receive management attention, particularly for controlling non-point sources.

Conclusions and Implications for Lake Erie load reduction

Controlling eutrophication in large, shallow lakes is a challenge because TP retention is a result of a delicate balance between settling and resuspension which in turn can be influenced by changes in water levels and meteorological conditions, and subject to substantial inter-annual variability. Based on our results for this large, shallow lake, Lake St. Clair is a net sink for

nutrients and this attenuation capacity can modify the magnitude and seasonal dynamics of nutrient loads. Contrary to the general assumption that tributary inflows and nutrient loads in large shallow polymictic (vertically well-mixed) systems are homogenously mixed and equally and proportionally exported to the lake's outflow and further downstream, we showed that spatial and temporal variation in tributary loads are important. The fact that the lake retains 35% of its DRP input (this study) and, on average, 20% of its TP load (Scavia et al., 2019), that the retention rates are highly dependent on winds (this study), and that there are differences in the retention rates for different tributaries are important considerations when allocating load reductions to Lake Erie.

There are many shallow water bodies around the world similar to Lake St. Clair and showing signs of ongoing or accelerated eutrophication where our findings may be applied. Examples of such systems include, but not limited to, large shallow lakes (e.g. Lake Winnipeg, Lake Manitoba, western basin of Lake Erie) and numerous smaller lakes and reservoirs, including many shallow and productive lakes and reservoirs that are imbedded within larger watersheds and similarly process nutrients between upper and lower reaches.

Acknowledgements

This work was funded by the Fred A and Barbara M Erb Family Foundation grant number 903, the University of Michigan Graham Sustainability Institute, and the University of Waterloo's Lake Futures and Global Water Futures Project. We appreciate the help, insights and advice offered by the University of Michigan's Dave Schwab, Lynn Vaccaro, Awoke Dagnew, Colleen Long, Yu-Chen Wang, and Jennifer Read. We appreciate the data graciously provided by Debbie Burniston, Alice Dove, Sean Backus, Luis Leon, and Reza Valipour from Environment and Climate Change Canada, and Katie Stammler from the Essex Region Conservation Authority.

References

Bocaniov, S. A., & Scavia, D. (2018). Nutrient loss rates in relation to transport time scales in a large shallow lake (Lake St. Clair, USA – Canada): insights from a three-dimensional lake model. *Water Resources Research*, 54, 3825-3840.

Bocaniov, S. A., & Scavia, D. (2016). Temporal and spatial dynamics of large lake hypoxia: Integrating statistical and three-dimensional dynamic models to enhance lake management criteria. *Water Resources Research*, 52, 4247-4263.

Bocaniov, S. A., Leon, L. F., Rao, Y. R., Schwab, D. J., & Scavia, D. (2016). Simulating the effect of nutrient reduction on hypoxia in a large lake (Lake Erie, USA-Canada) with a three-dimensional lake model. *Journal of Great Lakes Research*, 42 (6), 1228–1240.

Bocaniov, S. A., Ullmann, C., Rinke, K., Lamb, K. G., & Boehrer, B. (2014a). Internal waves and mixing in a stratified reservoir: Insights from three-dimensional modeling. *Limnologica -Ecology and Management of Inland Waters*, 49, 52-67.

Bocaniov, S. A., Smith, R. E., Spillman, C. M., Hipsey, M. R., & Leon, L. F. (2014b). The nearshore shunt and the decline of the phytoplankton spring bloom in the Laurentian Great Lakes: insights from a three-dimensional lake model. *Hydrobiologia*, 731(1), 151-172.

Bridgeman, T. B., Chaffin, J. D., & Filbrun, J. E. (2013). A novel method for tracking western Lake Erie Microcystis blooms, 2002–2011. *Journal of Great Lakes Research*, 39, 83–89.

Burniston, D., Dove, A., Backus, S., & Thompson, A. (2018). Nutrient concentrations and loadings in the St. Clair River–Detroit River Great Lakes interconnecting channel. *Journal of Great Lakes Research*, 44, 398-411.

Charlton, M. N., Milne, J. E., Booth, W. G., & Chiocchio, F. (1993). Lake Erie offshore in 1990: restoration and resilience in the central basin. *Journal of Great Lakes Research*, 19(2), 291-309.

GLWQA (Great Lakes Water Quality Agreement) (2016). The United States and Canada adopt phosphorus load reduction targets to combat Lake Erie algal blooms. https://binational.net/2016/02/22/finalptargets-ciblesfinalesdep/Viewed 25 February 2016.

Dean, R. G., & Dalrymple, R. A. (1984). *Water wave mechanics for engineers and scientists*. Prentice Hall, Inc., Englewood Cliffs, New Jersey, ISBN 0-13-946038-1.

Hamilton, D. P., & Mitchell, S. F. (1996). An empirical model for sediment resuspension in shallow lakes. *Hydrobiologia*, 317/3, 209–220.

Hamilton, D., & Mitchell, S. (1997). Wave-induced shear stresses, plant nutrients and chlorophyll in seven shallow lakes. *Freshwater biology*, 38(1), 159-168.

Hawley, N., & Lesht, B. M. (1992). Sediment resuspension in lake St. Clair. *Limnology and oceanography*, 37(8), 1720-1737.

Hipsey, M. R., & Hamilton, D. P. (2008). Computational Aquatic Ecosystem Dynamics Model: CAEDYM v3. v3.3 Science Manual (DRAFT). Centre for Water Research (CWR), University of Western Australia.

Hipsey, M. R. (2008). The CWR computational aquatic ecosystem dynamics model CAEDYM. User Manual. Centre for Water Research (CWR), University of Western Australia.

Hu, Y., Scavia, D., & Kerkez, B. (2018). Are all data useful? Inferring causality to predict flows across sewer and drainage systems using Directed Information and Boosted Regression Trees. *Water Resources*, 145, 697-706.

IJC (International Joint Commission) (1978). Great Lakes Water Quality Agreement of 1978, with annexes and terms of reference, between the United States of America and Canada. IJC: Windsor, Ontario, Canada, November 22, 1978.

IJC (International Joint Commission) (2012). Great Lakes Water Quality Agreement 2012. Protocol amending the agreement between Canada and the United States of America on Great Lakes water quality. IJC: Windsor, Ontario, Canada, September 7, 2012.

IJC (International Joint Commission) (2017). Draft domestic action plans for achieving phosphorus reductions in Lake Erie. Available at Canada-United States collaboration for Great Lakes water quality website: https://binational.net/2017/03/10/dap-pan/

Karatayev, A. Y., Burlakova, L. E., Mehler, K., Bocaniov, S. A., Collingsworth, P. D., Warren, G., Kraus, R. T., & Hinchey, E. K. (2018). Biomonitoring using invasive species in a large lake: Dreissena distribution maps hypoxic zones. J. Great Lakes Res., 44(4), 639-649.

Kalcic, M. M., Kirchhoff, C., Bosch, N., Muenich, R. L., Murray, M., Griffith Gardner, J., & Scavia, D. (2016). Engaging stakeholders to define feasible and desirable agricultural conservation in western Lake Erie watersheds. *Environmental Science* & *Technology*, 50(15), 8135-8145.

Kestin, J., Sokolov, M., & Wakeham, W. A. (1978). Viscosity of liquid water in the range − 8 C to 150 C. *Journal of Physical and Chemical Reference Data*, 7(3), 941-948.

Lang, G. A., Morton, J. A., & Fontaine III, T. D. (1988). Total phosphorus budget for Lake St. Clair: 1975–80. *Journal of Great Lakes Research*, 14(3), 257-266.

Leon, L. F., Smith, R. E., Hipsey, M. R., Bocaniov, S. A., Higgins, S. N., Hecky, R. E., Antenucci, J. P., Imberger, J. A., & Guildford, S. J. (2011). Application of a 3D

hydrodynamic–biological model for seasonal and spatial dynamics of water quality and phytoplankton in Lake Erie. *Journal of Great Lakes Research*, 37(1), 41-53.

Liu, W., Bocaniov, S. A., Lamb, K. G., & Smith, R. E., 2014. Three dimensional modeling of the effects of changes in meteorological forcing on the thermal structure of Lake Erie. *Journal of Great Lakes Research*, 40(4), 827-840.

Ludsin, S. A., Kershner, M. W., Blocksom, K. A., Knight, R. L., & Stein, R. A. (2001). Life after death in Lake Erie: nutrient controls drive fish species richness, rehabilitation. *Ecological Applications*, 11(3), 731-746.

Maccoux, M. J., Dove, A., Backus, S. M., & Dolan, D. M. (2016). Total and soluble reactive phosphorus loadings to Lake Erie: A detailed accounting by year, basin, country, and tributary. *Journal of Great Lakes Research*, 42, 1151-1165.

Masselink, G., Hughes, M., & Knight, J. (2014). *Introduction to Coastal Processes and Geomorphology*. Routledge.

Michalak, A. M., Anderson, E. J., Beletsky, D., Boland, S., Bosch, N. S., Bridgeman, T. B., Chaffin, J. D., Cho, K., Confesor, R., Daloğlu, I. and DePinto, J. V. (2013). Record-setting algal bloom in Lake Erie caused by agricultural and meteorological trends consistent with expected future conditions. *Proceedings of the National Academy of Sciences*, 201216006.

Muenich, R. L., Kalcic, M., & Scavia, D. (2016). Evaluating the impact of legacy P and agricultural conservation practices on nutrient loads from the Maumee River watershed. *Environmental Science* & *Technology*, 50(15), 8146-8154.

Nalepa, T. F., Gardner, W.S., & Malczyk, J. M. (1991). Phosphorus cycling by mussels (Unionidae: Bivalvia) in Lake St. Clair. *Hydrobiologia*, 219(1): 239-250.

Nalepa, T. F., Hartson, D.J., Gostenik, G. W., Fanslow, D. L., & Lang, G. A. (1996). Changes in the freshwater mussel community of Lake St. Clair: from Unionidae to Dreissena polymorpha in eight years. *Journal of Great Lakes Research*, 22(2), 354-369.

Oveisy, A., Rao, Y. R., Leon, L. F., & Bocaniov, S. A. (2014). Three-dimensional winter modeling and the effects of ice cover on hydrodynamics, thermal structure and water quality in Lake Erie. *Journal of Great Lakes Research*, 40, 19-28.

Scavia, D., Allan, J. D., Arend, K. K., Bartell, S., Beletsky, D., Bosch, N. S., Brandt, S. B., Briland, R. D., Daloğlu, I., DePinto, J. V., Dolan, D. M., Evans, M. A., Farmer, T. M., Goto, D., Han, H., Höök, T. O., Knight, R., Ludsin, S. A., Mason, D., Michalak, A. M., Richards, R. P., Roberts, J. J., Rucinski, D. K., Rutherford, E., Schwab, D. J., Sesterhenn, T., Zhang, H., & Zhou, Y. (2014) Assessing and addressing the re-eutrophication of Lake Erie: Central basin hypoxia. *Journal of Great Lakes Research*, 40(2), 226-246.

Scavia, D., DePinto, J. V., & Bertani, I. (2016). A Multi-model approach to evaluating target phosphorus loads for Lake Erie. *Journal of Great Lakes Research*, 42, 1139-1150.

Scavia, D., Kalcic, M., Muenich, R. L., Read, J., Aloysius, N., Bertani, I., Boles, C., Confesor, R., DePinto, J., Gildow, M., & Martin, J. (2017). Multiple models guide strategies for agricultural nutrient reductions. *Frontiers in Ecology and the Environment*, 15(3), 126-132.

Scavia, D., Bocaniov, S. A., Dagnew, A., Long, C. M., & Wang, Y.-C. (2019). St. Clair - Detroit River system: Phosphorus mass balance and implications for Lake Erie load reduction, monitoring, and climate change. *Journal of Great Lakes Research*, 45, 40-49.

Schwab, D. J., Clites, A. H., Murthy, C. R., Sandall, J. E., Meadows, L.A., & Meadows, G. A., 1989. The effect of wind on transport and circulation in Lake St. Clair. *Journal of Geophysical Research*: *Oceans*, 94(C4), 4947-4958.

Soulsby, R. L. (1983). The bottom boundary layer of shelf seas. In *Elsevier oceanography series* (Vol. 35, pp. 189-266). Elsevier.

Tanaka, M., Girard, G., Davis, R., Peuto, A., & Bignell, N. (2001). Recommended table for the density of water between 0 C and 40 C based on recent experimental reports. *Metrologia*, 38(4), 301-309.

Tsai, C. H., & Lick, W. (1986). A portable device for measuring sediment resuspension. *Journal of Great Lakes Research*, 12(4), 314-321.

Zhou, Y., Michalak, A. M., Beletsky, D., Rao, Y. R., & Richards, R. P. (2015). Record-breaking Lake Erie hypoxia during 2012 drought. *Environmental Science* & *Technology*, 49(2), 800-807.

Table 1. Long term (1918 – 2017) monthly mean water levels for Lake St. Clair (meters; IGLD85*) and corresponding mean lake water volumes (km^3), mean and maximum depths (m)**.

Month	Mean Value
Jan	174.84
Feb	174.79
Mar	174.90
Apr	175.04
May	175.13
Jun	175.18
Jul	175.20
Aug	175.16
Sept	175.09
Oct	175.00
Nov	174.91
Dec	174.91
Mean Water Level* (m):	175.01
Mean Volume** (km^3):	4.3
Mean Depth** (m):	3.9
Max Depth** (m):	6.4

*IGLD85 is a Low Water Datum for Lake St. Clair referenced to IGLD85 (174.4 m).
** Calculations were based on the bathymetric map of Lake St. Clair and water level measurements at the three water level gauging stations (Table ST-1; Fig. 1a): #9034052, # 9044049, and #11965.

Table 2. Characterization of the sub-watersheds within St. Clair River – Lake St. Clair (SCR-LSC) system.

#	System Component	Watershed Area (km^2)			As % of the entire SCR -LSC system
		USA	Canada	Total	
1	St. Clair River*	2,997	502	3,499	22.7
2	Lake St. Clair, including:	2,727	9,181	11,908	77.3
2.1	Clinton River	2,064	-	2,064	13.4
2.2	Thames River	-	5,875	5,875	38.1
2.3	Sydenham River	-	2,676	2,676	17.4
2.4	other tributaries	663	630	1,293	8.4
3	Total	5,724	9,683	15,407	100
4	As % of the SCR – LSC system	37.2	62.8	100	

* the upstream watershed of the St. Clair River arising from the drainage of the upper Laurentian Great Lakes (Lakes Superior, Michigan and Huron) is 576,014 km^2 and not included in the table.

Table 3. Average flows and total loading (March 1 to October 30 inclusive) of total phosphorus (TP) and dissolved reactive phosphorus (DRP) in metric tonnes (MT) for various tributaries to Lake St. Clair for the base case scenario (Table 4).

#	Tributary Name	Total TP load (MT)	Total DRP Load (MT)	Daily Flow ($m^3 s^{-1}$)	As % of Total Lake Input		
					TP (%)	DRP (%)	Tributary inflow (%)
1	St. Clair River	1507.873	448.551	5384.696	78.13	71.88	97.762
2	Thames River	200.873	70.835	68.412	10.41	11.35	1.242
3	Sydenham River	72.785	27.799	28.418	3.77	4.45	0.516
4	Clinton River	89.520	48.224	19.393	4.64	7.73	0.352
5	Ruscom River	3.603	2.018	0.818	0.19	0.32	0.015
6	Belle River	2.368	1.326	0.538	0.12	0.21	0.010
7	Pike Creek	2.024	1.134	0.460	0.10	0.18	0.008
8	Salt River	5.570	4.568	1.385	0.29	0.73	0.025
9	Puce River	1.559	0.873	0.354	0.08	0.14	0.006
10	Little River	2.475	1.386	0.562	0.13	0.22	0.010
11	Swan Creek	1.318	1.028	1.021	0.07	0.16	0.019
12	Beauben Creek	2.528	2.199	0.796	0.13	0.35	0.014
13	Little Ceek	1.397	0.782	0.317	0.07	0.13	0.006
14	Moison Creek	0.515	0.288	0.117	0.03	0.05	0.002
15	Marsac Creek	0.844	0.692	0.318	0.04	0.11	0.006
16	Duck Creek	0.441	0.247	0.100	0.02	0.04	0.002
17	Crapaud Creek	0.786	0.645	0.296	0.04	0.10	0.005
	Atmospheric load	33.428	11.430	36.983	1.73	1.83	0.671
	Total:	1929.907	624.025				

Table 4. Meteorological forcing scenarios represented by the base case scenario (scenario B) and eight additional scenarios (C1 to C8) using the same initial, boundary and forcing (inflow-outflow) conditions as in case B except for the meteorological forcing indicative of those observed during a particular year.

Scenario #	Meteorological forcing conditions (year)	Scenario details and modifications made relative to the base case scenario (Scenario B):
Base case (B)	2009	Base case scenario B (model calibrated for 2009)
C1	1995	Different meteorological conditions indicative of 1995
C2	1996	Different meteorological conditions indicative of 1996
C3	2003	Different meteorological conditions indicative of 2003
C4	2005	Different meteorological conditions indicative of 2005
C5	2008	Different meteorological conditions indicative of 2008
C6	2010	Different meteorological conditions indicative of 2010
C7	2012	Different meteorological conditions indicative of 2012
C8	2014	Different meteorological conditions indicative of 2014

Table 5. Retention of total phosphorus (R_{TP}) from March 1 to October 30 inclusive under different meteorological forcing scenarios. Retention is determined as the difference between TP entering and leaving the lake (TP_IN and TP_OUT). MT means metric tonnes.

Scenario	Season average air temperature	Season average wind speed	Total Phosphorus (TP)			
			TP_IN	TP_OUT	R_{TP}	R_{TP}
	$(\overline{AT})$	$(\overline{WS})$	(MT)	(MT)	(MT)	(%)
	(°C)	(m s^{-1})				
Base case (B)	15.37	6.02	1929.907	1596.9	333.01	17.26
C1	15.71	6.44	1929.907	1632.7	297.21	15.40
C2	14.72	6.59	1929.907	1672.9	257.01	13.32
C3	14.80	6.03	1929.907	1585.1	344.81	17.87
C4	16.74	5.82	1929.907	1530.0	399.91	20.72
C5	15.72	5.91	1929.907	1550.6	379.31	19.65
C6	17.20	6.04	1929.907	1567.1	362.81	18.80
C7	17.41	6.09	1929.907	1563.7	366.21	18.98
C8	15.19	6.12	1929.907	1608.2	321.71	16.67
				Average:	340.22	17.63

Table 6. Retention of total dissolved phosphorus (R_{DRP}) from March 1 to October 30 inclusive under different meteorological forcing scenarios. Retention is determined as the difference between amount of DRP entering and leaving the lake (DRP_IN and DRP_OUT). MT means metric tonnes.

Scenario	Season average air temperature	Season average wind speed	Dissolved Reactive Phosphorus (DRP)			
	$(\overline{AT})$ (°C)	$(\overline{WS})$ (m s^{-1})	DRP_IN (MT)	DRP_OUT (MT)	R_{DRP} (MT)	R_{DRP} (%)
Base case (B)	15.37	6.02	624.025	406.9	217.125	34.79
C1	15.71	6.44	624.025	410.2	213.825	34.27
C2	14.72	6.59	624.025	423.0	201.025	32.21
C3	14.80	6.03	624.025	409.6	214.425	34.36
C4	16.74	5.82	624.025	397.0	227.025	36.38
C5	15.72	5.91	624.025	407.4	216.625	34.71
C6	17.20	6.04	624.025	404.0	220.025	35.26
C7	17.41	6.09	624.025	403.2	220.825	35.39
C8	15.19	6.12	624.025	398.7	225.325	36.11
				Average:	217.358	34.83

Table 7. Simple and multiple ordinary least squared (OLS) regression models relating retention of total phosphorus (R_{TP}; MT) and dissolved reactive phosphorus (R_{DRP}; MT) to explanatory variables such as season averaged values of air temperature ($\overline{AT}$; °C) and wind speed ($\overline{WS}$; m s^{-1}) for simulation scenarios listed in Table 4 (N = 9).

Model	Dependent variable	Regression	R^2	P-value
1	R_{TP}	(1370.08** ±140.74) - (168.34** ±22.99)·[$\overline{WS}$]	0.885	<0.001
2	R_{TP}	(-109.09 ±199.54) + (28.31 ±12.55)·[$\overline{AT}$]	0.421	0.059
3	R_{TP}	(1013.63** ±129.96) - (145.16** ±15.29)·[$\overline{WS}$] + (13.52* ±3.73)·[$\overline{AT}$]	0.964	<0.001
4	R_{DRP}	(364.15** ±45.49) – (23.99* ±7.43)·[$\overline{WS}$]	0.601	0.014
5	R_{DRP}	(149.78** ±37.56) + (4.26 ±2.37)·[$\overline{AT}$]	0.317	0.114
6	R_{DRP}	(306.23** ±68.24) – (20.23* ±8.03)·[$\overline{WS}$] + (2.20 ±1.96)·[$\overline{AT}$]	0.668	0.037
7	R_{DRP}	(172.25** ±14.46) + (0.13* ±0.04)·[R_{TP}]	0.585	0.016

* significant at the $0.01 < P \leq 0.05$ level; ** significant at the $P < 0.01$ level; ± standard errors of the regression parameters; R^2, coefficient of determination; N, number of observations; for the multiple regressions, the independent variables are listed in a decreasing order of explained variance; MT, metric tonnes.

Table 8. The allocation of lake bottom areas for various depth zones in Lake St. Clair.

Depth range (meters)	Bottom Area (km^2)	As % of total lake bottom (%)
0 – 0.9	102	9.2
1 – 1.9	170	15.3
2 – 2.9	90	8.1
3 – 3.9	179	16.1
4 – 4.9	246	22.1
5 – 5.9	287	25.8
6 – 6.4	40	3.6
Total:	1114	100

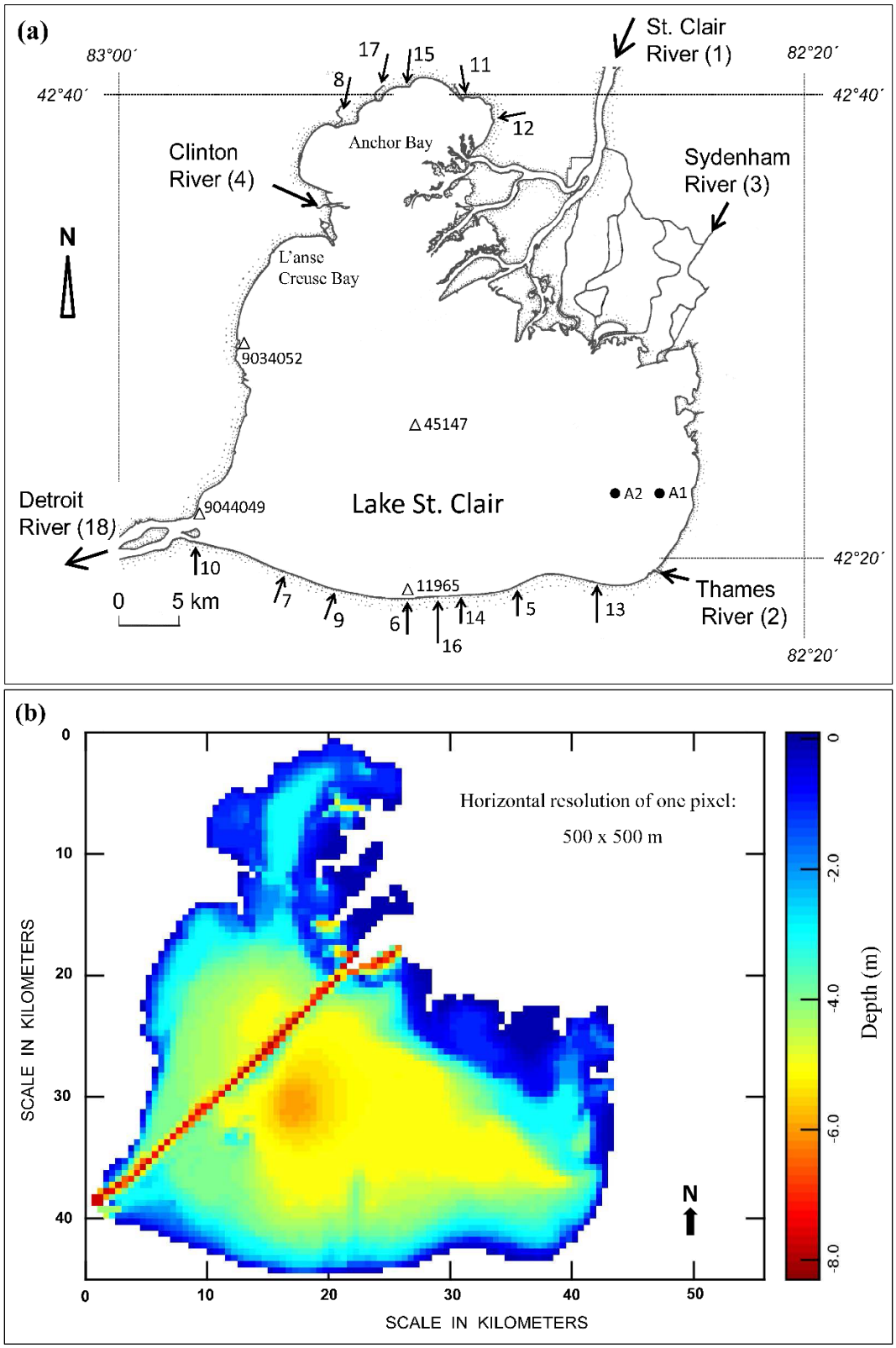

Figure 1. (a) Map of Lake St. Clair with the lake outflow, Detroit River, and 17 included tributaries indicated by arrows with numbers corresponding to their names in Table 3. Open triangle in the

idicate the locations of in-lake buoy (#45147) and wtare level gauging stations, while solid circles show the deployment locations of instrumented tripods in 2016 (stations A1-2), (b) Bathymetric map of Lake St. Clair. The deep channel dissecting lake from north to southwest is the navigational channel.

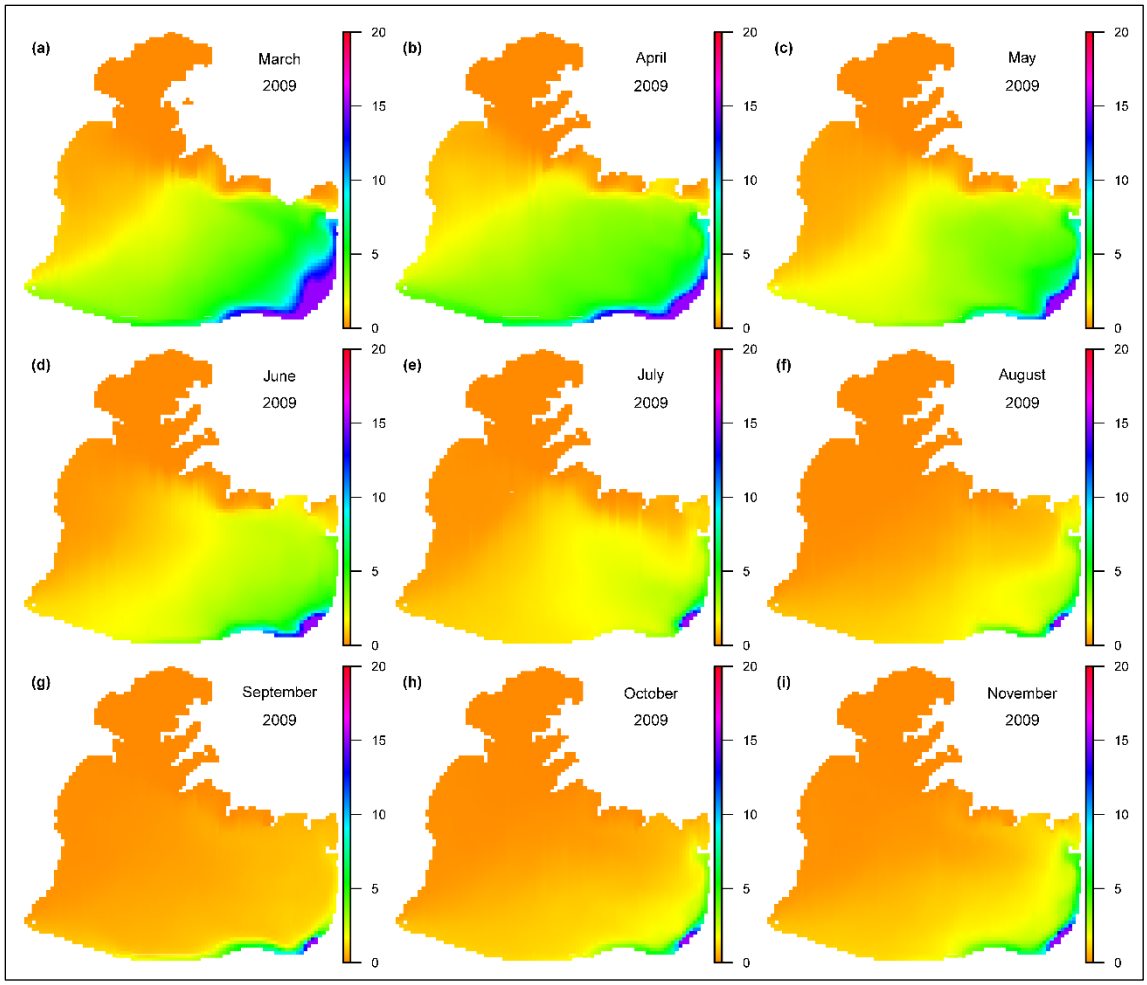

Figure 2. Maps showing spatial and temporal distribution of the Thames River water at the lake surface (depth: 0.2 m) expressed as a percent of the original Thames River water (monthly-averaged value).

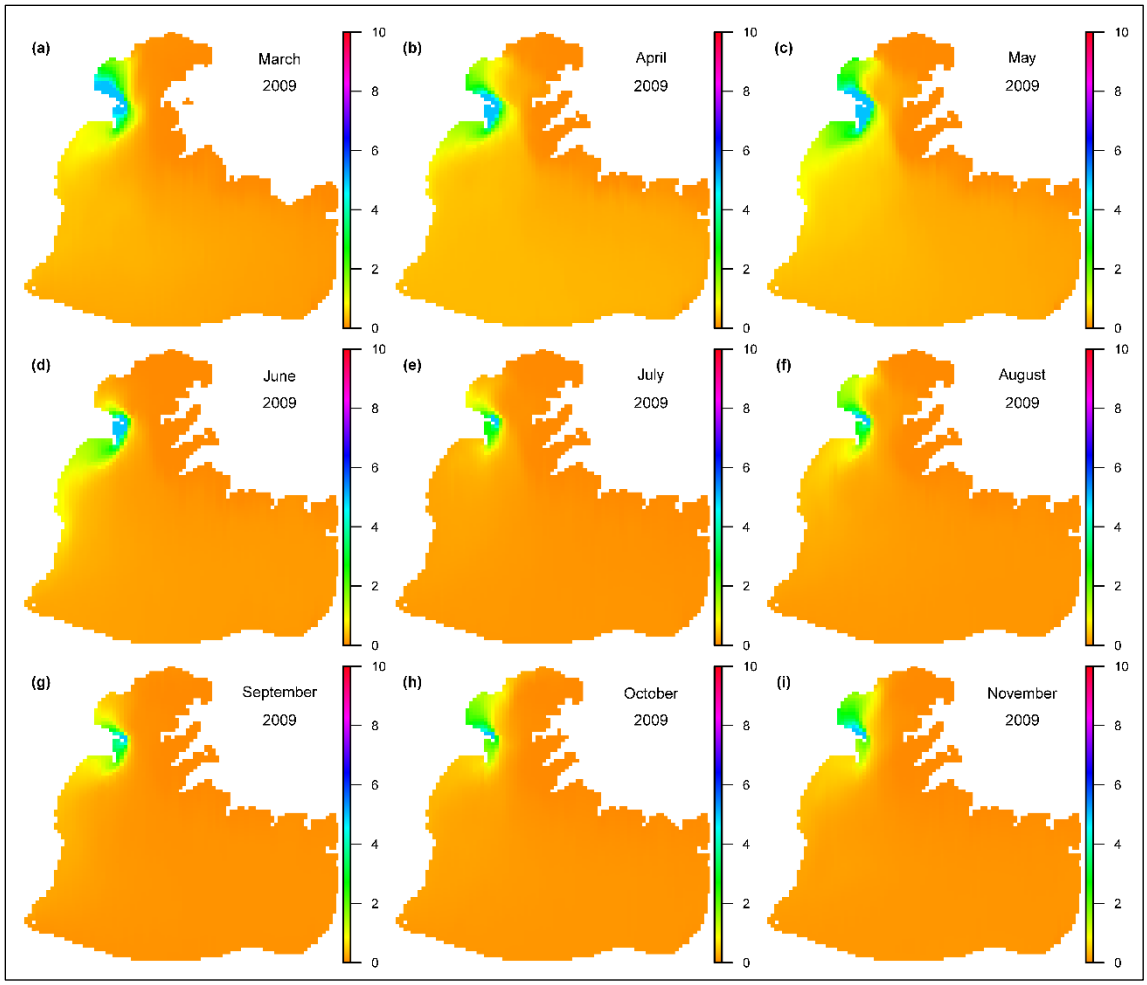

Figure 3. Maps showing spatial and temporal distribution of the Clinton River water at the lake surface (depth: 0.2 m) expressed as a percent of the original Clinton River water (monthly-averaged value).

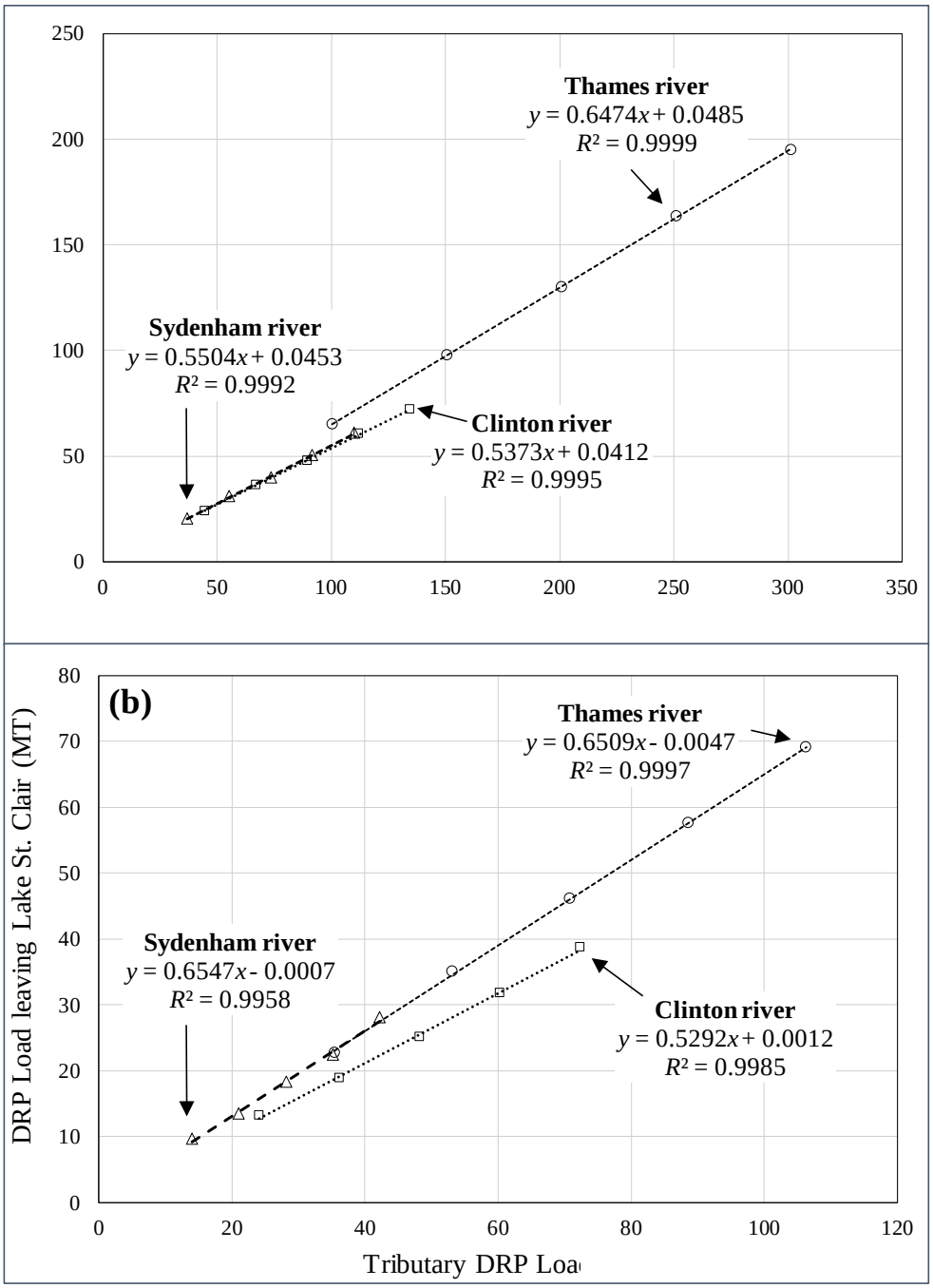

Figure 4. Lake St. Clair outflow response curves for three major tributaries: (a) for total phosphorus - TP; and, (b) for dissolved Reactive Phosphorus - DRP. Please note that the regression intercepts were subtracted from the full load leaving Lake St. Clair (*y*-axis), and MT stands for metric tonnes.

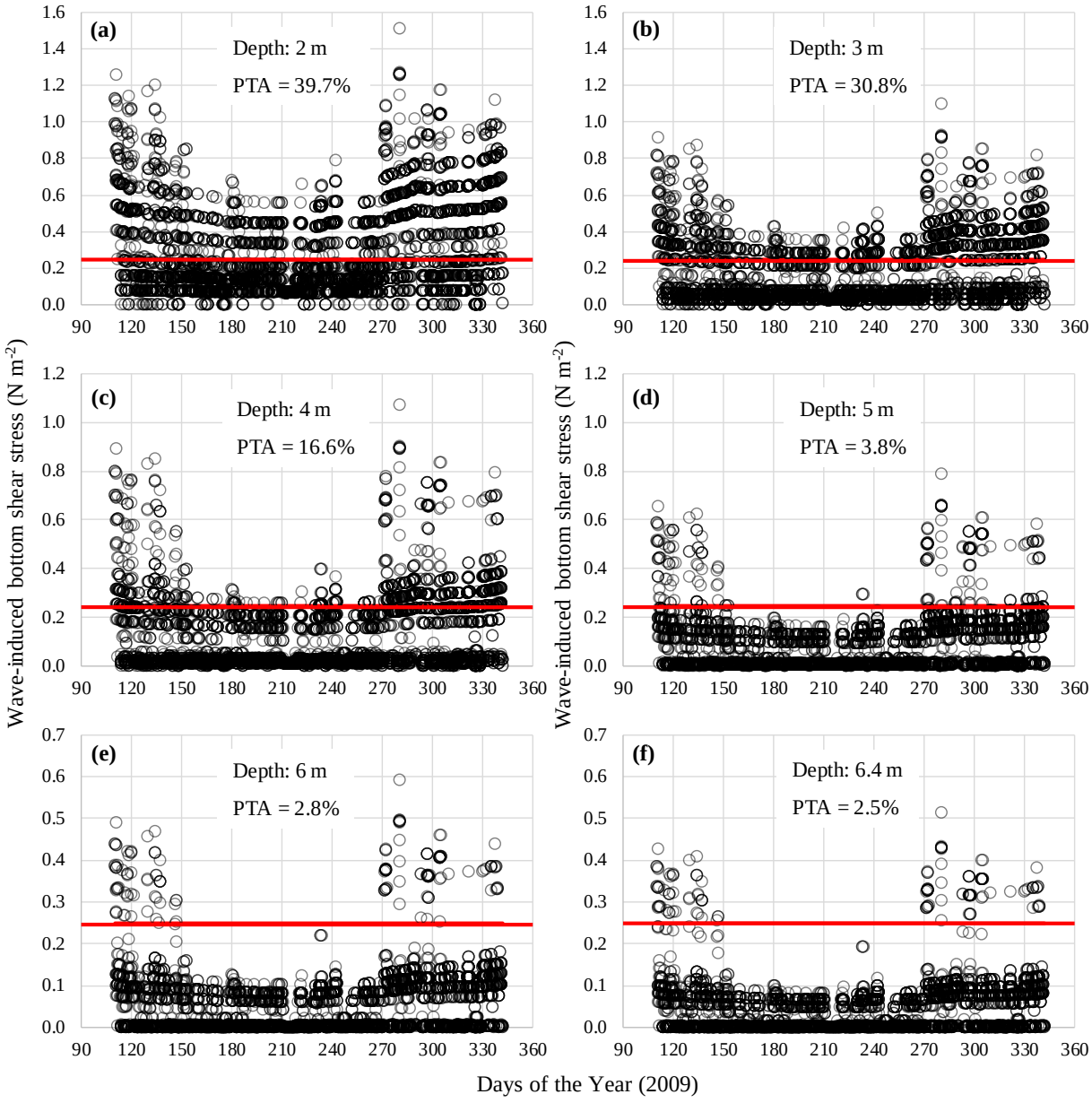

Figure 5. Wave-induced hourly bottom shear stress (τ_w; N m^{-2}) calculated for the lake bottom at different depths: (a) 2 m; (b) 3 m; (c) 4 m; (d) 5 m; (e) 6 m; and, (f) 6.4 m. The data used in calculations (significant wave height and wave period) are based on hourly observations in 2009 at the in-lake buoy # 45147 (Fig. 1a). Open circles and darker shaded area indicate percent of daily lake ice cover in 2009, while lighter shaded area indicate values of hourly bottom shear stress which are below the critical value (τ_{crit}) of 0.25 N m^{-2} (Tsai and Lick, 1986). PTA indicates the percent of the entire time when $\tau_w > \tau_{crit}$

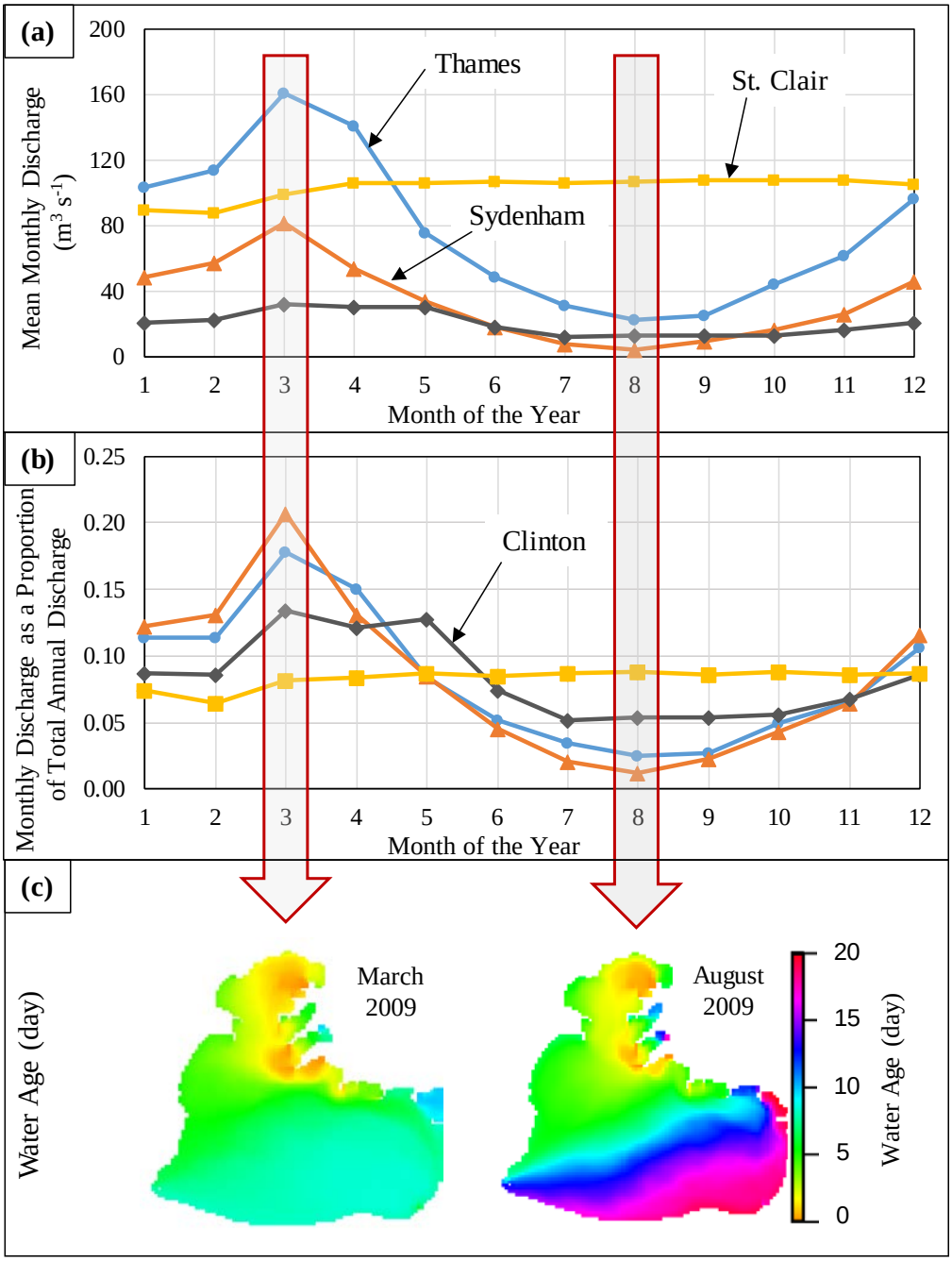

Figure 6. (a) Mean monthly discharges averaged from 2000 to 2017 for the St. Clair River (yellow squares) and three major tributaries: Thames (blue circles), Sydenham (brown triangles), and Clinton (black diamonds) rivers. (b) Mean monthly discharge as a proportion of total annual discharge over the period 2000 through 2017 for the same rivers as in (a). (d) Lake St. Clair water age in May and August 2009 estimated by Bocaniov and Scavia (2018).

Supporting Information (SI) for

On the role of a large shallow lake (Lake St. Clair, USA-Canada) in modulating phosphorus loads to Lake Erie

Serghei A. Bocaniov[1, 2,*], Philippe Van Cappellen[2], and Donald Scavia[3]

[1] Graham Sustainability Institute, University of Michigan, Ann Arbor, Michigan, USA.
[2] Department of Earth and Environmental Sciences, University of Waterloo, Waterloo, Ontario, Canada.
[3] School for Environment and Sustainability, University of Michigan, Ann Arbor, Michigan, USA.

*Corresponding author: bocaniov@umich.edu

Contents of this file:

Introduction:

The supporting information material has eighteen pages and provides additional information used in the main paper and is organized in the graphical and tabled forms consisting of two supporting tables (ST-1 and ST-2) and twelve supporting figures (SF-1 to SF-12).

List of Tables:

List of Figures:

List of Figures (*Continued from previous page*):

Table ST-1. Summary of dates and locations of in-lake buy, water level gauging stations, and tripods deployments in Lake St. Clair (Fig. 1a).

St. No	Latitude Longitude	Location	Period of Deployment		Agency*	Station designation
			From	To		
45147	42°25′48″N 82°40′48″W	Central Lake St. Clair	20.04.2009	03.12.2009	ECCC	wave buoy
11965	42°20′26.2″N 82°33′03.7″W	Belle River, Ontario	continues	continues	ECCC	water level
9034052	42°28.4' N 82°52.8' W	St. Clair Shores, Michigan	continues	continues	NOAA	water level
9044049	42°21.4' N 82°55.8' W	Windmill Point, Michigan	continues	continues	NOAA	water level
A1	42°23′32.7″N 82°27′06.8″W	South-eastern Lake St. Clair	27.04.2016	03.11.2016	ECCC	ADCP
A2	42°20′26.2″N 82°33′03.7″W	South-eastern Lake St. Clair	27.04.2016	08.11.2016	ECCC	ADCP

* ECCC, Environment and Climate Change Canada; ANL, Argonne National Laboratory; NOAA, National Oceanic and Atmospheric Administration.

Table ST-2. Monthly mean current velocity ±SD (cm s^{-1}) of near-bottom currents for the ADCP deployments in 2016 at the locations A1 and A2 (Fig. 1a; Table ST-1).

Month	A1	A2
	Velocity	Velocity
May	3.6 ±1.9	4.8 ±3.9
Jun	2.8 ±1.6	4.7 ±3.0
Jul	2.2 ±1.3	3.1 ±1.7
Aug	1.9 ±1.1	2.7 ±1.5
Sept	2.0 ±1.1	2.8 ±1.7
Oct	2.3 ±1.4	3.9 ±2.8
Grand Mean	2.5 ±1.5	3.7 ±2.7

* Note: the estimates of monthly values for April and November were omitted from the results as the available measurements are only for about three days (Apr 27-30 and Nov 1-3).

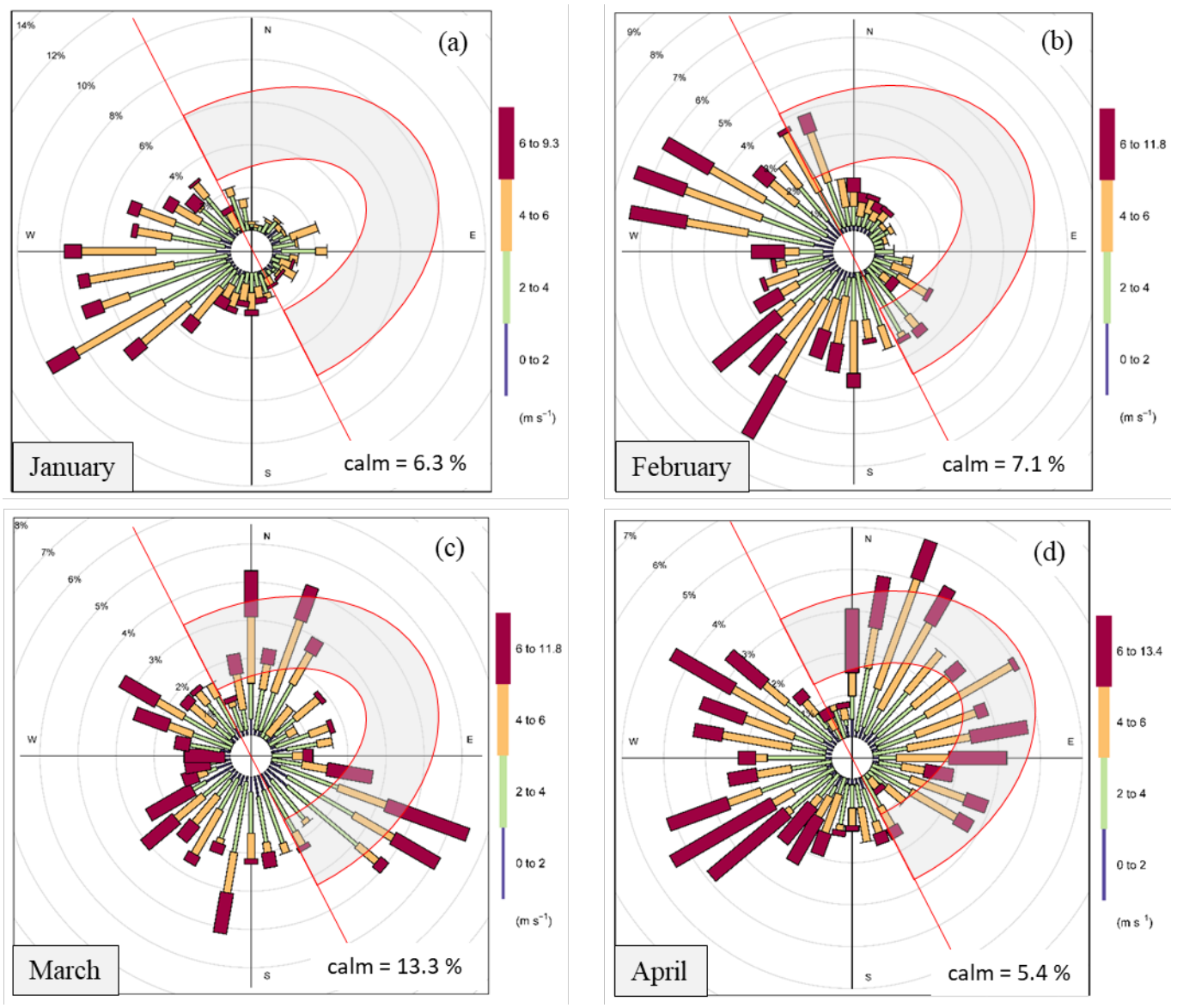

Figure SF-1. Wind rose diagrams showing atmospheric wind characteristics (frequency, speed, direction) for January (a), February (b), March (c) and April (d) for the wind conditions observed in 2009 at Detroit City AP meteorological station. Wind rose diagrams for other years are typical to the shown one, as for example those in 2010 (Fig. SF-4). Wind directions favoring the short water residence time for the Thames River (Fig. SF-12a –d) are indicated by the grey semi-circle.

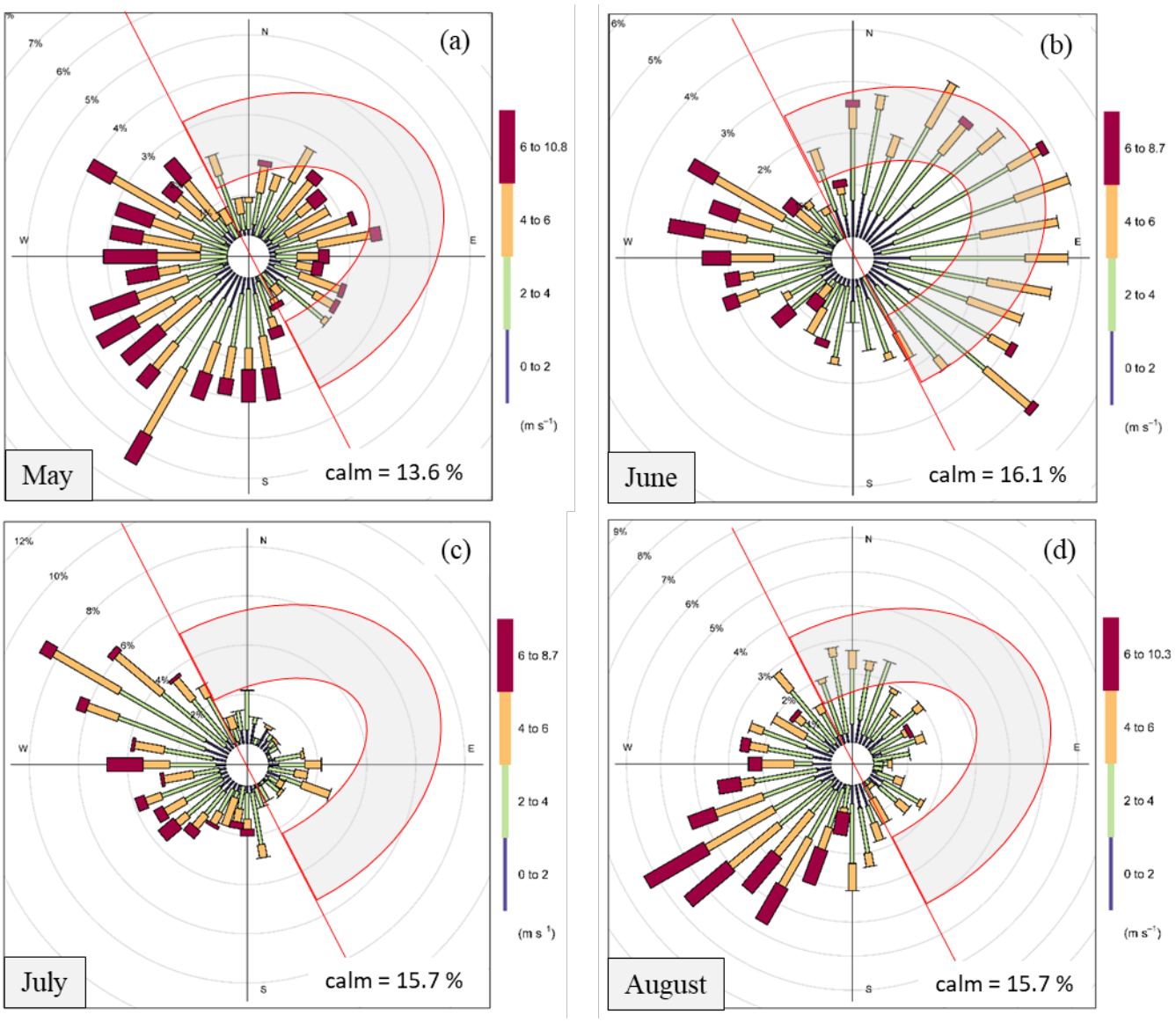

Figure SF-2. Wind rose diagrams showing wind characteristics (frequency, speed, direction) for May (a), June (b), July (c) and August (d) for the wind conditions observed in 2009 at the Detroit City AP meteorological station. Wind rose diagrams for other years are typical to the shown one, as for example that in 2010 (Fig. SF-5). Winds favoring the short water residence time for the Thames River (Fig. SF-12a –d) are indicated by the grey semi-circle.

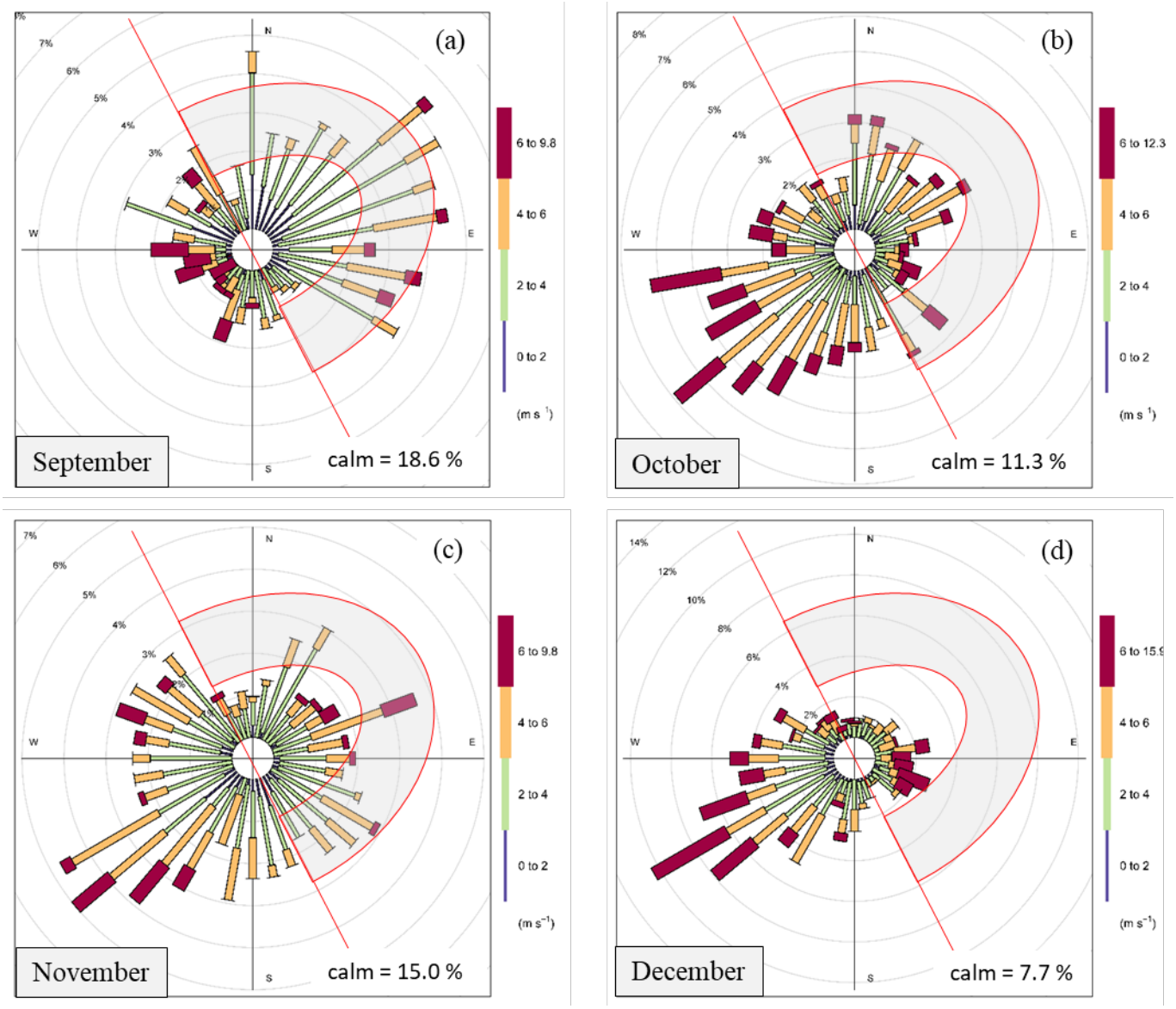

Figure SF-3. Wind rose diagrams showing the frequency, speed, and direction of winds for September (a), October (b), November (c) and December (d) for the wind conditions observed in 2009 at Detroit City AP meteorological station. Wind rose diagrams for other years are typical to the shown one, as for example that in 2010 (Fig. SF-6). Wind directions favoring the short water residence time for the Thames River (Fig. SF-12a –d) are indicated by the grey semi-circle.

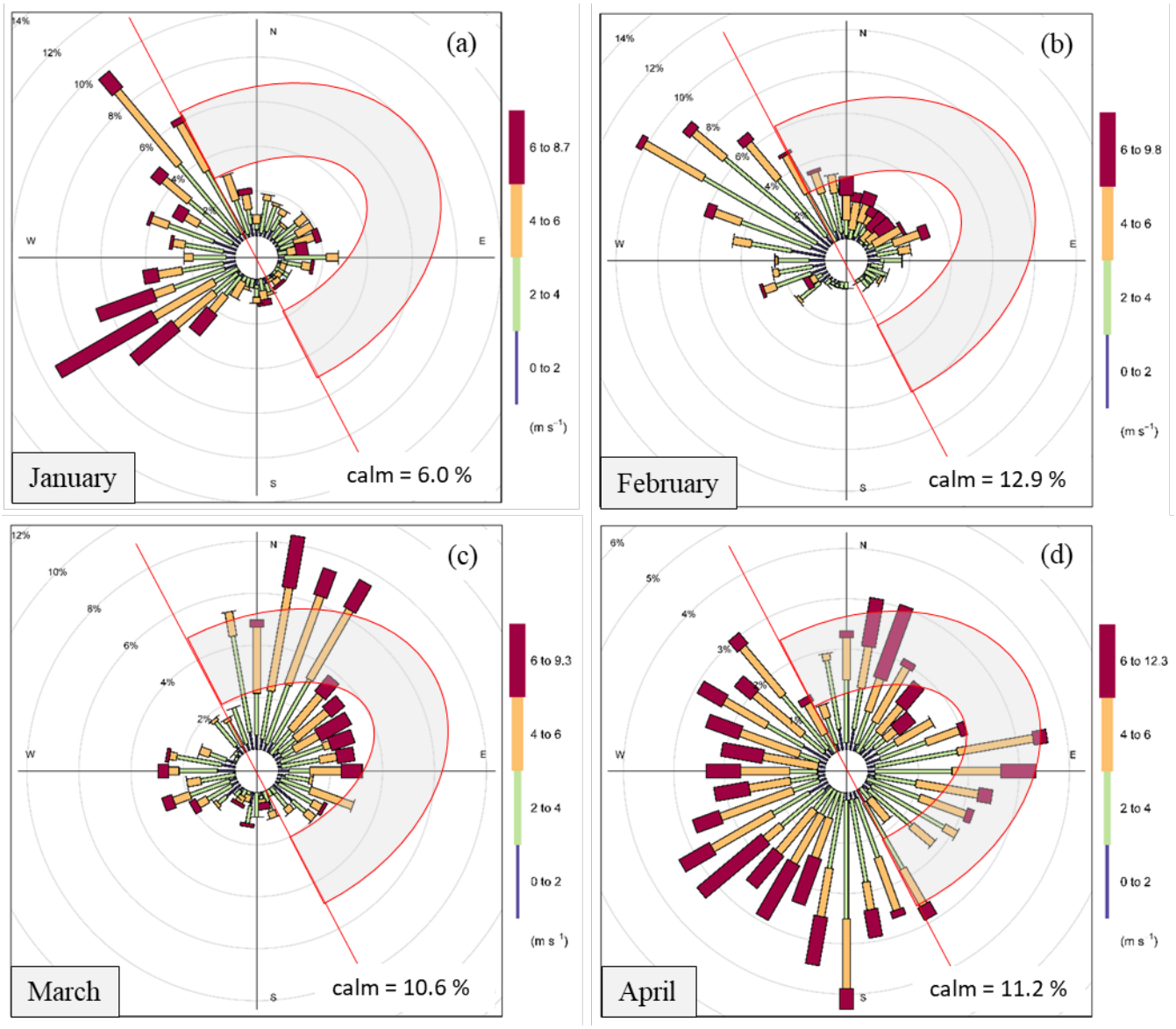

Figure SF-4. Wind rose diagrams showing atmospheric wind characteristics (frequency, speed, direction) for January (a), February (b), March (c) and April (d) for the wind conditions observed in 2010 at Detroit City AP meteorological station. Wind directions favoring the short water residence time for the Thames River (Fig. SF-12a –d) are indicated by the grey semi-circle.

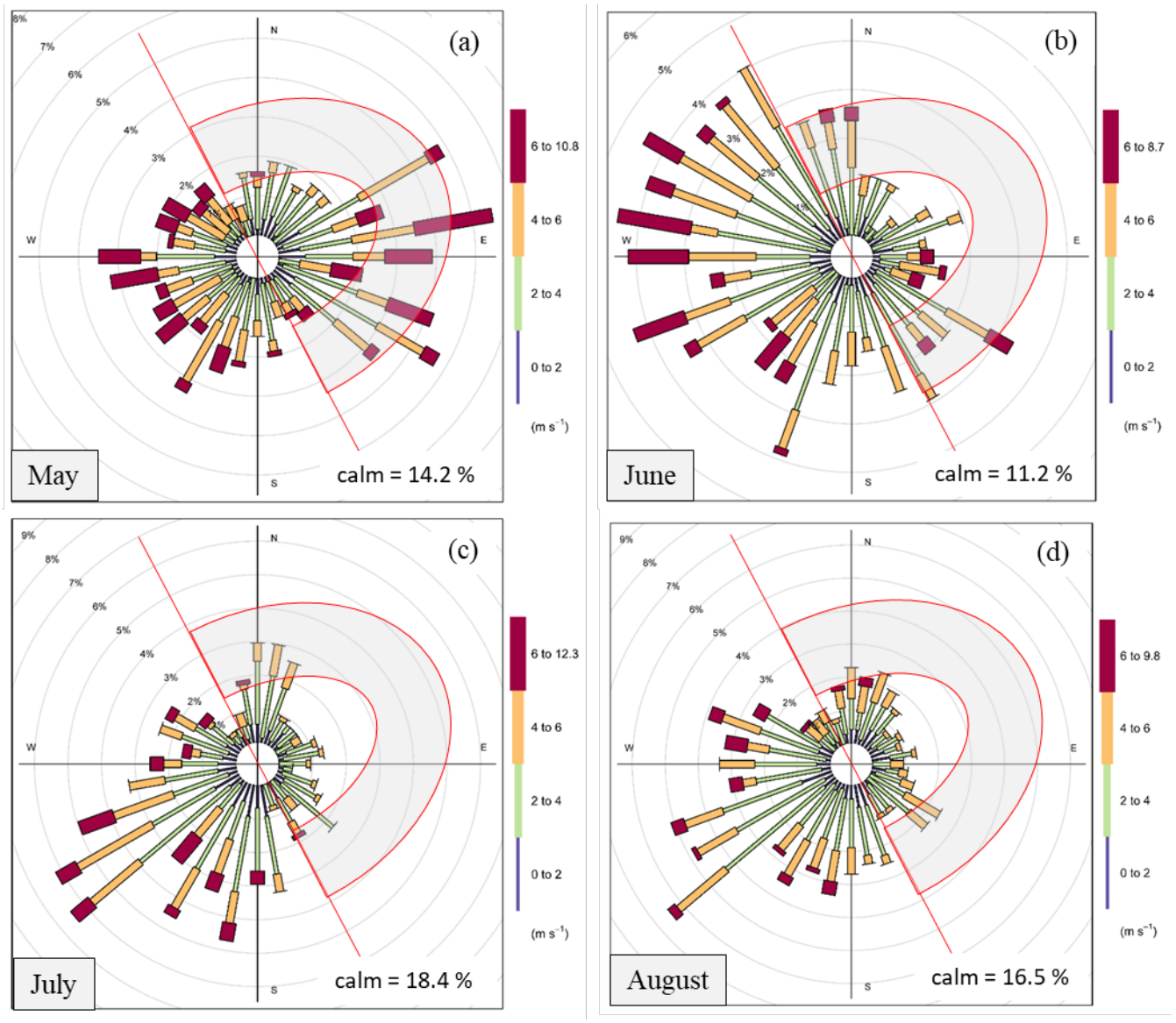

Figure SF-5. Wind rose diagrams showing wind characteristics (frequency, speed, direction) for May (a), June (b), July (c) and August (d) for the wind conditions observed in 2010 at the Detroit City AP meteorological station. Wind directions favoring the short water residence time for the Thames River (Fig. SF-12a –d) are indicated by the grey semi-circle.

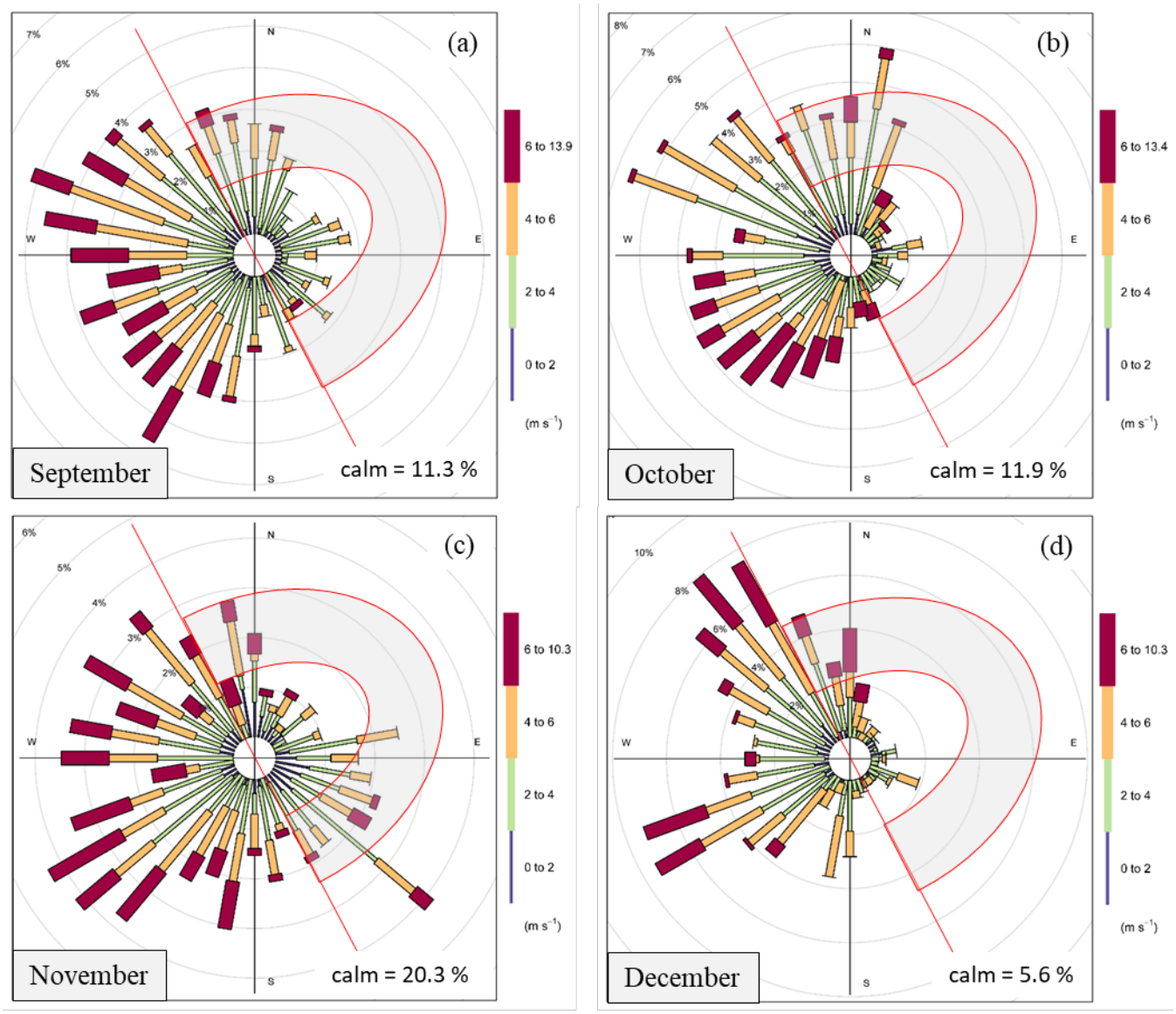

Figure SF-6. Wind rose diagrams showing the frequency, speed, and direction of winds for September (a), October (b), November (c) and December (d) for the wind conditions observed in 2010 at Detroit City AP meteorological station. Wind directions favoring the short water residence time for the Thames River (Fig. SF-12a –d) are indicated by the grey semi-circle.

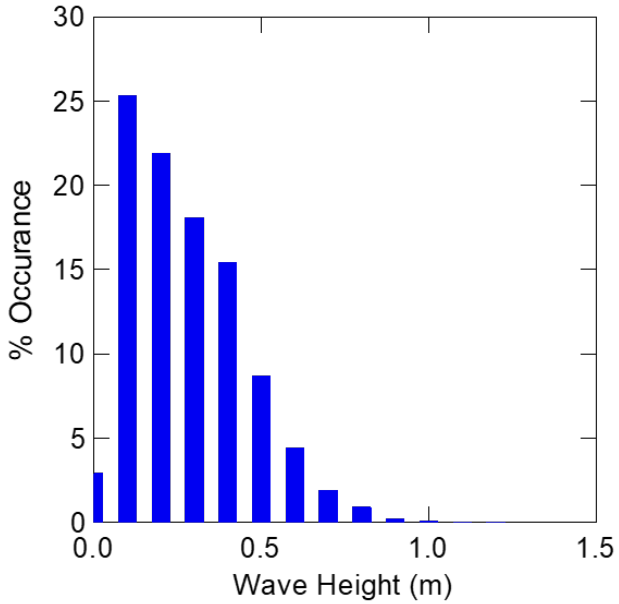

Figure SF-7. Percent distribution histogram of measured wave heights from April 20 to December 7, 2009, at buoy #45147 (Fig. 1a; Table ST-1).

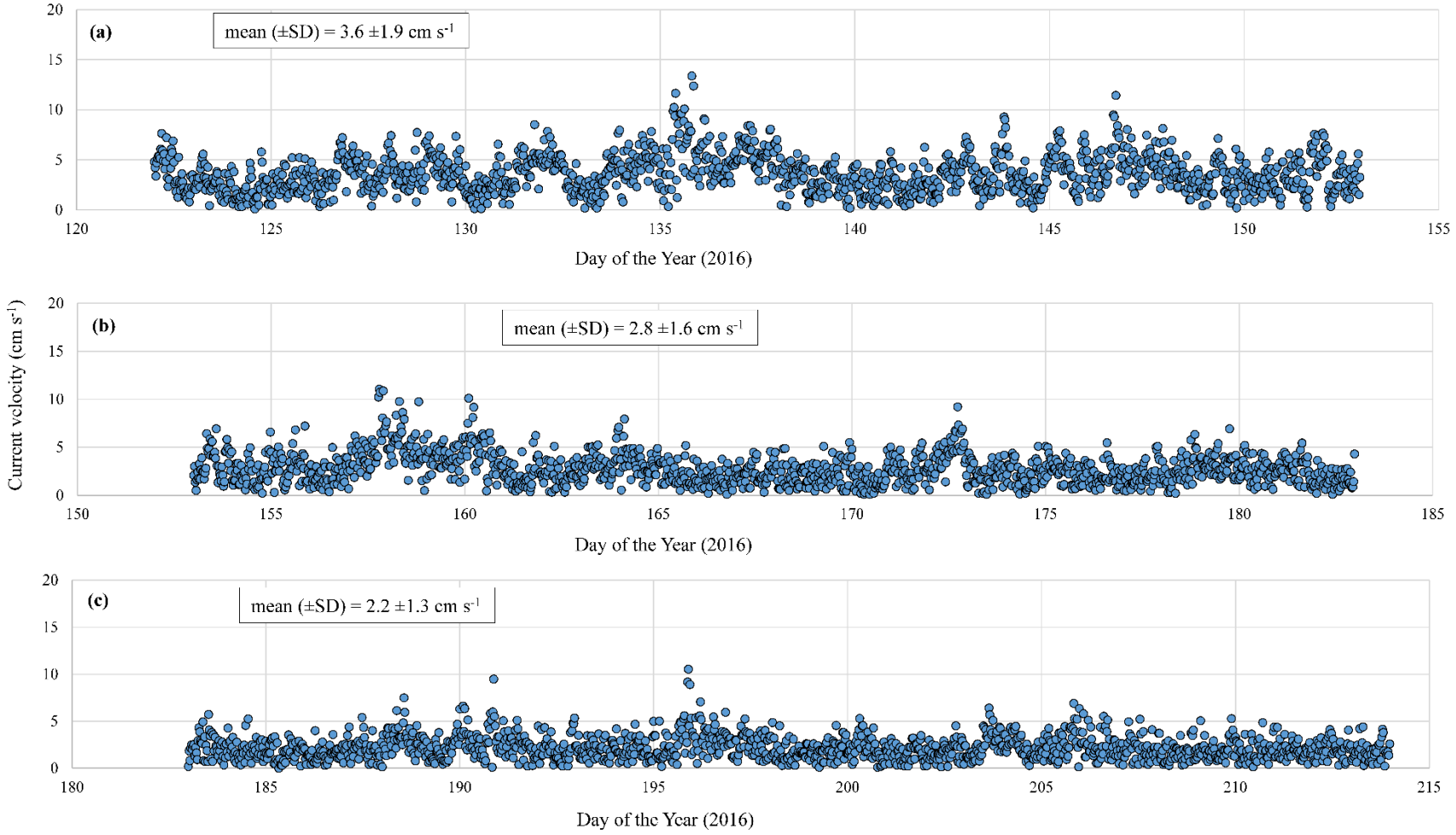

Figure SF-8. Current velocities at elevation of 1.46 m above bottom recorded every 30 min at station A1 (Fig. 1a; Table ST-1) in 2016 and shown for (a) May, (b) June, and (c) July.

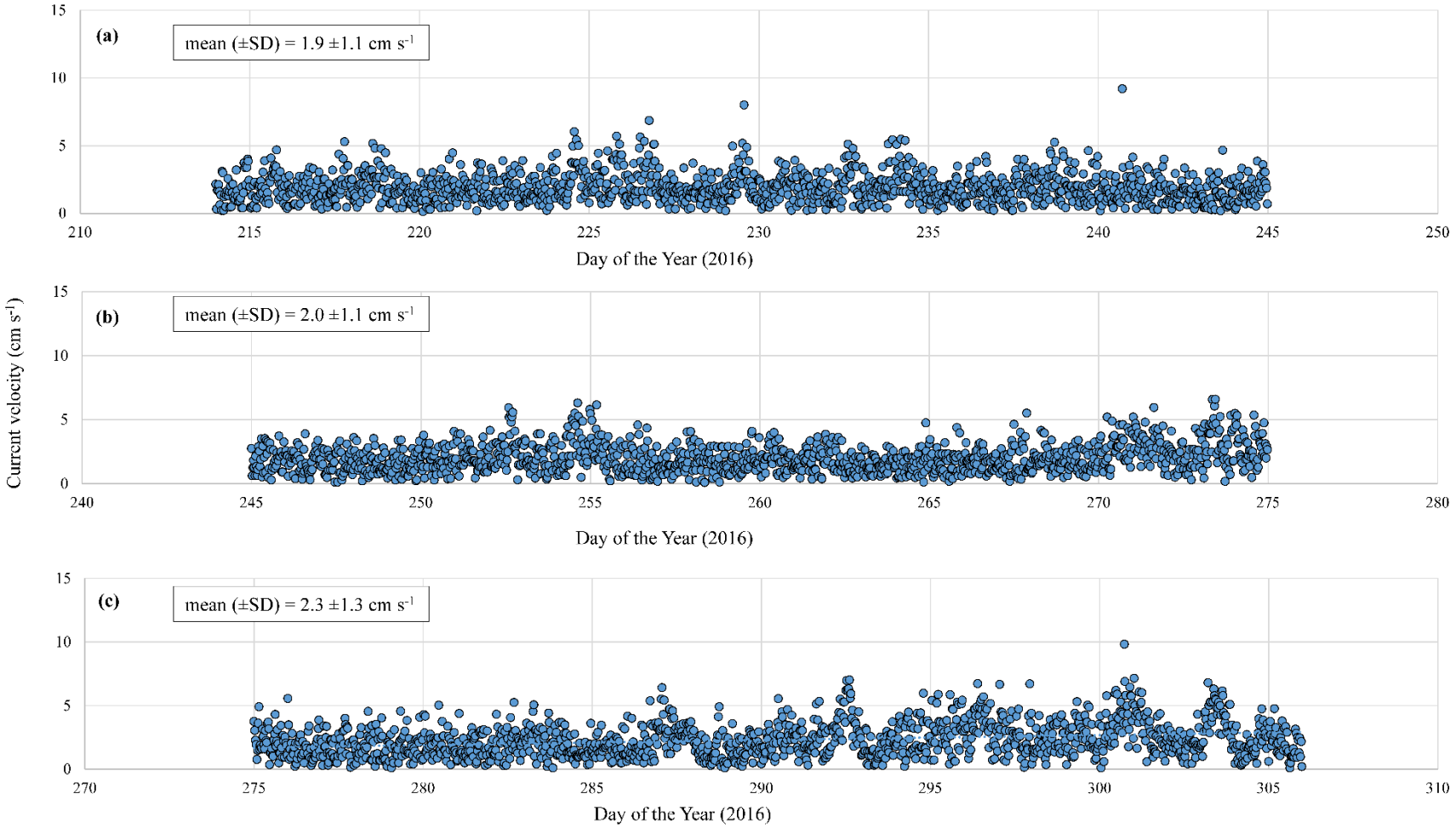

Figure SF-9. Near-bottom current velocities at elevation of 1.46 m above bottom recorded every 30 min at station A1 (Fig. 1a; Table ST-1) in 2016 and shown for (a) August, (b) September, and (c) October.

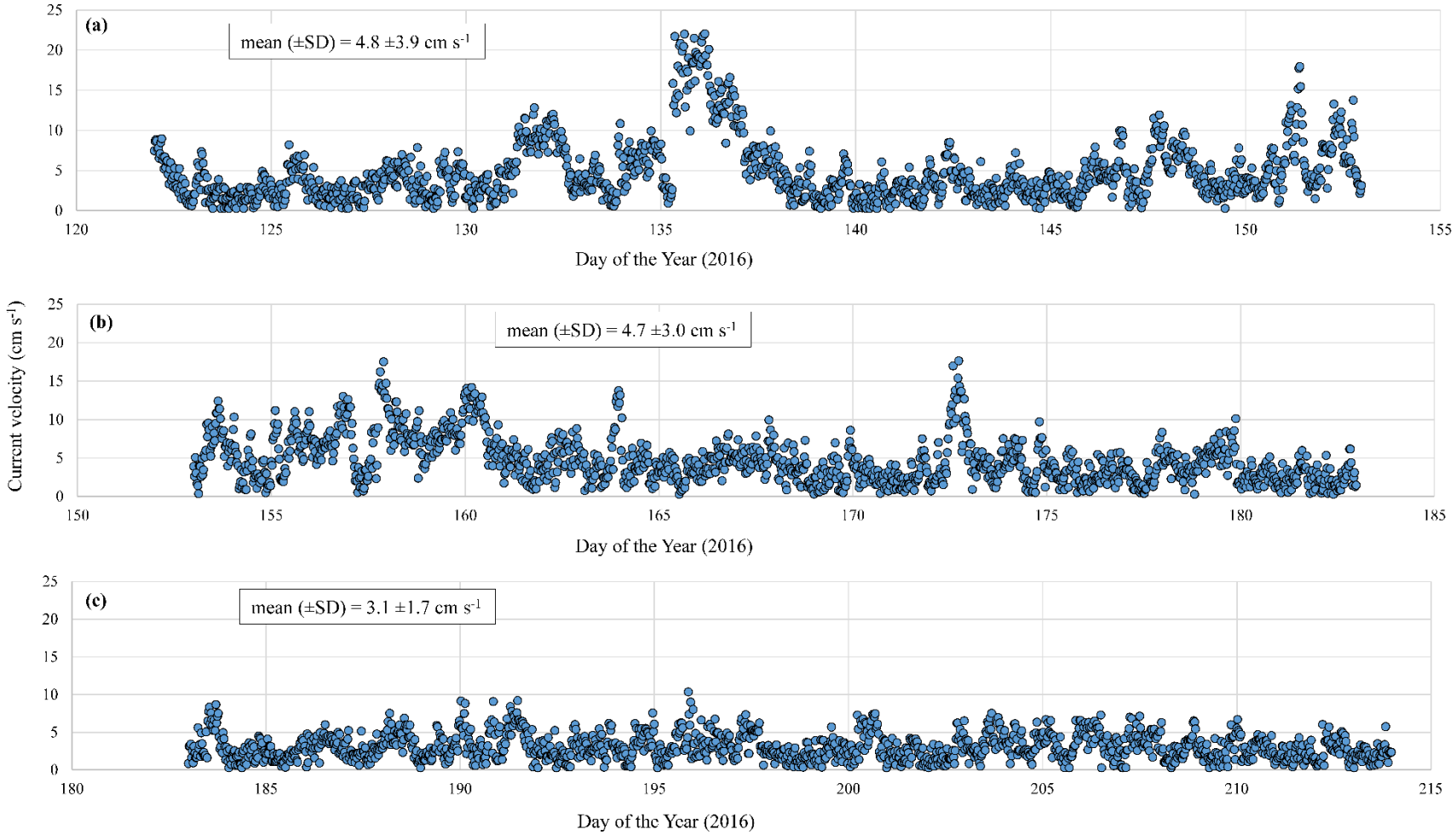

Figure SF-10. Near-bottom current velocities at elevation of 1.46 m above bottom recorded every 30 min at station A2 (Fig. 1a; Table ST-1) in 2016 and shown for (a) May, (b) June, and (c) July.

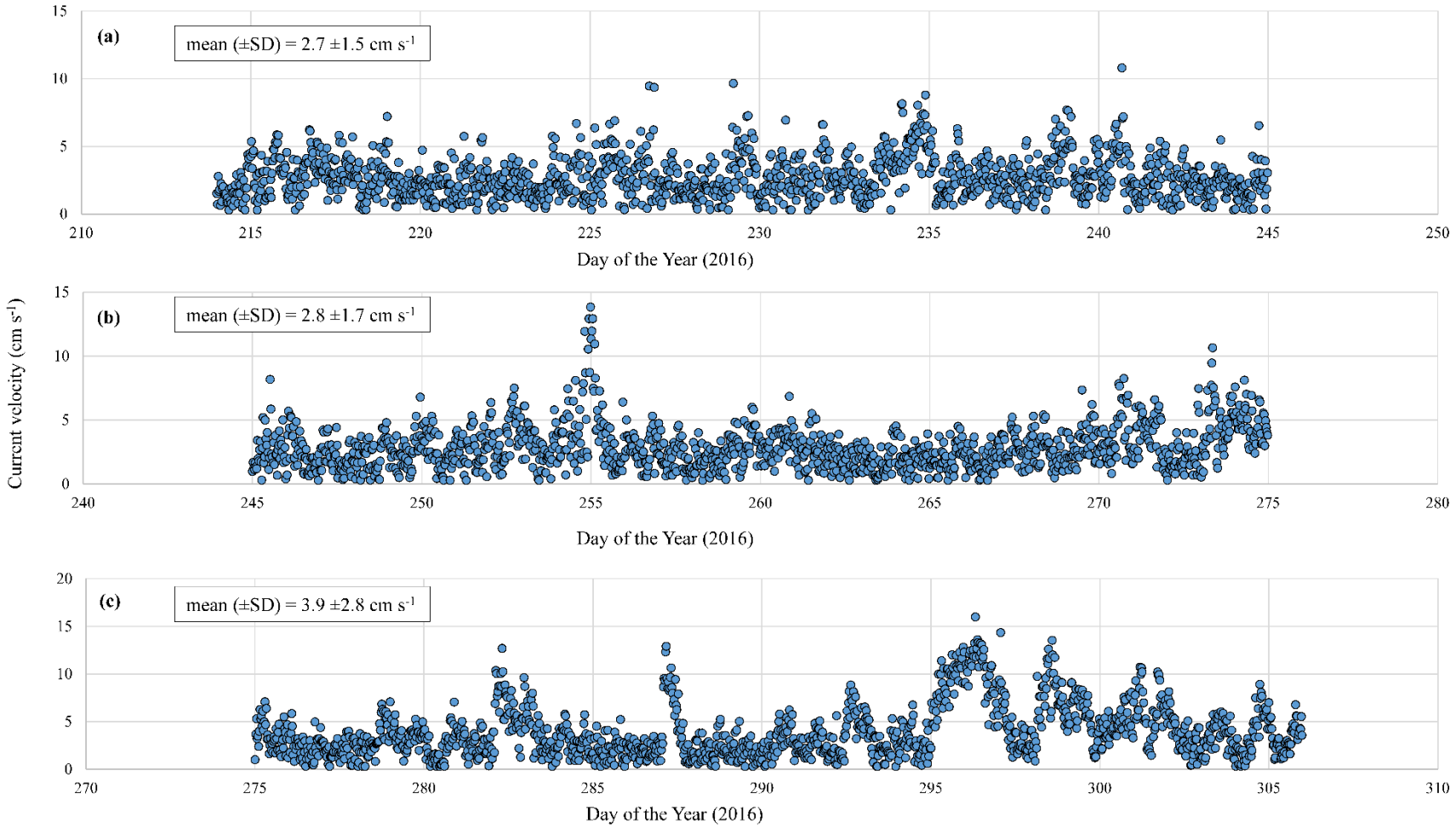

Figure SF-11. Current velocities at elevation of 1.46 m above bottom recorded every 30 min at station A2 (Fig. 1a; Table ST-1) in 2016 and shown for (a) August, (b) September, and (c) October.

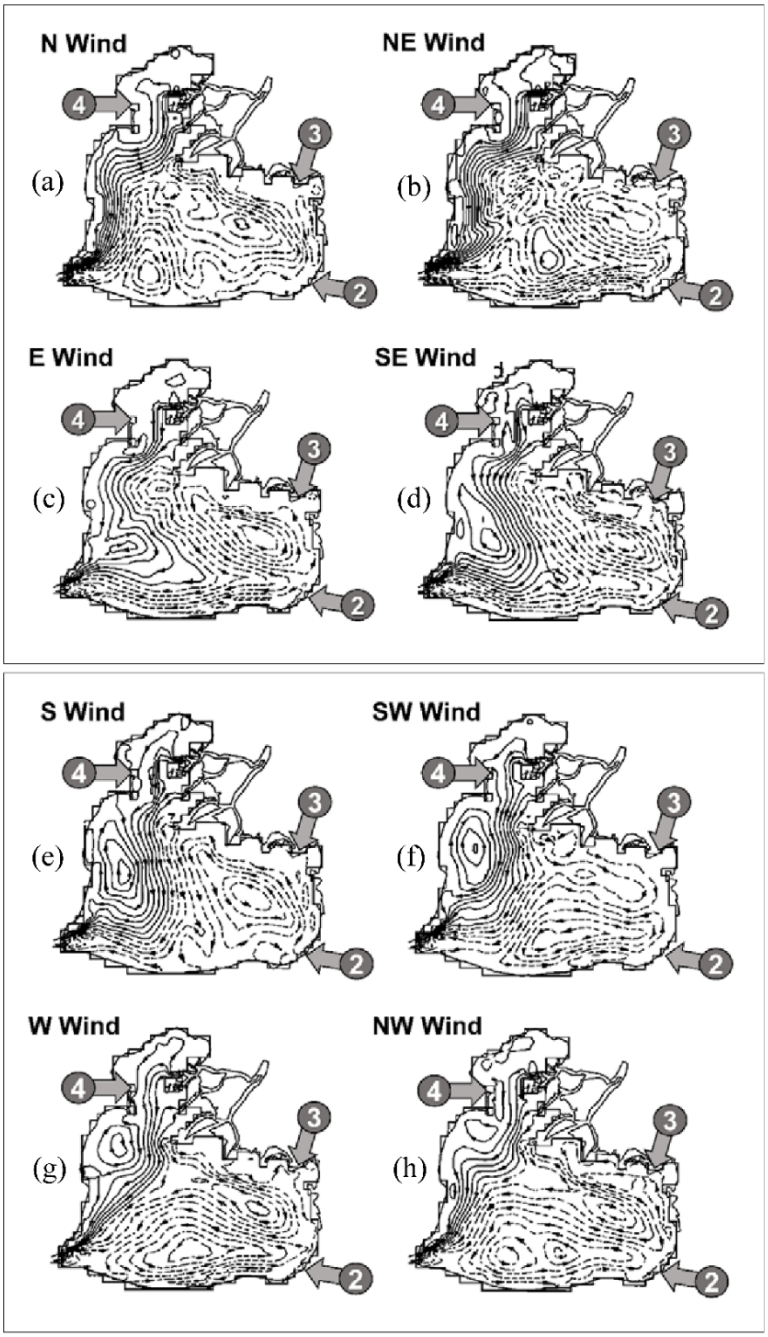

Figure SF-12. Lake St. Clair circulation patterns (vertically averaged) under conditions of various wind directions (modified from Schwab et al., 1981): (a) northern winds; (b) north-western wind; (c) eastern winds; (d) south-eastern winds; (e) southern winds; (f) south-western winds; (g) western winds; and, (h) north-western winds. The numbers indicate three major tributaries: Thames River (2), Sydenham River (3), and Clinton River (4). Thin arrows show the direction of water movement. Wind directions favoring the shorter residence time for the Thames River water mass are shown in the upper panel (a, b, c, d), and those favoring longer retention time are shown in the lower panel (e, f, g, h).

11